Досліджено вплив нерегульованого електроприводу змінного струму і регульованого електроприводу постійного струму головних насосів сухого доку на мережу суднобудівельного заводу «Океан» (Україна) в середовищі MatLab SimPowerSystems.

Задля точного моделювання глибокопазних асинхронних двигунів було застосовано власну методику визначення параметрів Т-подібної схеми заміщення і коефіцієнту в'язкого тертя віртуального двигуна за каталожними даними. Ця методика спирається на формули, які відповідають Т-подібній і уточненій Г-подібній схемі заміщення. Запропоновано ввести в розрахунок скореговані значення кратності початкового пускового і критичного моменту. Номінальний коефіцієнт потужності визначається опосередковано та порівнюється із каталожним значенням. Залежності роторних опорів апроксимовані елементарними функціями, які забезпечують майже сталі значення цих параметрів при докритичних значеннях ковзання.

В результаті моделювання стало зрозуміло, що навіть при почерговому пусканні нерегульованих електронасосних агрегатів відбувається істотне падіння напруги в мережі.

Математичну модель електроприводів постійного струму було побудовано зі спільною двоконтурною системою автоматичного керування частотою обертання. На вході кожного генератору імпульсів керування включено резонансний фільтр, чим виключаються можливі помилки в роботі.

Результати моделювання переконують у тому, що під час роботи електроприводів постійного струму в мережі виникають комутаційні перепади напруги, споживаний струм виявляється суттєво несинусоїдальним та відбувається споживання реактивної енергії. З урахуванням паразитної ємності кабельної лінії виникають високочастотні коливання напруги, що створює небезпеку для роботи електрообладнання.

Завдяки використанню фільтро-компенсуючого пристрою перераховані негативні явища можуть бути виключені, тоді електропривод постійного струму за багатьма показниками переважатиме нерегульований асинхронний електропривод. Для мінімізації споживання реактивної енергії може слугувати система автоматичного керування з інтегральним регулятором потужності реактору зі змінним коефіцієнтом підсилення

Ключові слова: асинхронний двигун, каталожні дані, постійний струм, ПІ-регулятор, питома ємність, фільтро-компенсуючий пристрій

UDC 621.313.04
DOI: 10.15587/1729-4061.2019.177837

ANALYSIS OF THE INFLUENCE OF DRYDOCK MAIN PUMPS DRIVE ON ELECTRIC NETWORK

P. Khristo
Senior Lecturer
Department of Electromechanical Engineering
Odessa National Polytechnic University
Shevchenka ave., 1,
Odessa, Ukraine, 65044
E-mail: Pavel.John.Khristo@gmail.com

Received date 11.06.2019
Accepted date 20.08.2019
Published date 28.10.2019

1. Introduction

An integral part of many shipbuilding and ship-repair yards are drydocks or wet dock chambers. Among the first ones, the docks having lightweight gravity drainage chambers on the basis are known as the most widespread, which is explained by less stringent hydrogeological conditions and capital costs for construction. Ground water pressure on the structural elements of dock chambers of this type is partially or completely eliminated by drainage over the base area and/or waterproofing. During operation, dock chambers are periodically filled and emptied for the purpose of docking or undocking the vessel, including operations of preparing a keel-block set and precise fit prior to repair works. Drydocks are serviced by own pump stations, usually located in the main chamber section. Four main groups of pumps ensure normal operation of dock emptying and water supply systems. Drainage pumps serve to remove groundwater pressure on the dock structural elements. The main pumps remove the water prism from the chamber to the adjacent water area (minimum pumping level is limited by funneling and penetration of air in the emptying system). Stripping pumps are used for the final drainage of the chamber when the main pumps are switched off and also to remove production, rain and drainage water. Production pumps are responsible for technical water supply and fire safety of the dock [1, 2]. Capacities of the main and stripping or drainage pumps differ by about an order of magnitude. Thus, the major energy consumers at the stations are the main pumps, which in most cases are equipped with direct-on-line unadjustable-speed induction motor drive. Meanwhile, in [3, 4] it is shown that by switching to adjustable-speed drive of the main pumps, it is possible to achieve significant energy savings in the process of chamber emptying. In addition, it is possible to adjust the supply at the stage of final guidance of the vessel before fitting on the dock set and at low levels of water table in the chamber. The need for regulating pressure valves and/or switching off and restarting part of the main pumps is eliminated.

It is known that squirrel-cage induction motors used in electric drives have enhanced starting characteristics due to the round-slot rotor cage [5]. This increases the starting torque ratio, but the starting current ratio is still large enough. As a consequence, a rather long transient process caused by significant joint inertia of the electric drive may be accompanied by a marked decrease in supply voltage. The latter phenomenon in most cases adversely affects the

operation of other electric equipment and requires quantitative analysis. Using adjustable-speed DC drive, it is possible to achieve a significant reduction in the starting current and the corresponding sag of the finite-power supply. But there is a problem of influence of current harmonics on the electric network generated by the thyristor converter, and distortion of voltage, which powers other electric consumers.

The urgency of the work consists in reduction of the influence of powerful electric drives of the drydock main pumps on the network of the shipbuilding and ship-repair yard and providing the possibility of speed control of the main pumps.

2. Literature review and problem statement

The reliability of the results of induction motor drive start-up simulation largely depends on the accuracy of setting the parameters of the mechanics and equivalent circuit of the motor [6]. Such data, especially for large variable-parameter electric machines, are rarely contained in reference books or directories and need to be exactly defined [7]. For this purpose, the procedure of identification according to the results of experimental tests is carried out, as, in particular, in the autotuning of intelligent frequency converters, or only computing methods are used, when experimental studies are impossible [8, 9]. The first direction is developing more intensively, but the second one has not exhausted itself, although a lot of printed works, in particular [10–13], are devoted to determining the parameters of the induction motor equivalent circuit based on reference data. However, the methods of approximate estimation described in them have both advantages and disadvantages. So, in accordance with [10], it is proposed to look for the parameters of the induction motor equivalent circuit in a rather unusual way when these values are considered as functions of some auxiliary variable, but recommendations for determining its proper value have no strict theoretical justification. The estimation procedure given in [11, 12] is correct for motors with constant parameters. In the case of heavy-duty deep-bar or double-squirrel cage induction motors (in both cases, parameters are variable), this procedure is unsuitable as it leads to a significant error of results. Besides, there is an additional source of estimation error, which causes the distortion of results, even with unchanged equivalent circuit parameters. The reason for the additional error lies in the fact that some formulas have an approximate value of critical slip equal to the greater of the roots of a quadratic equation – a consequence of the simplified Kloss formula. The work [13] contains formulas obtained for machines with variable parameters, but they are inferior to other methods in the accuracy of results, including that reported in [10]. It is important to emphasize that the variable nature of rotor resistance in this case does not coincide with the exact analytical solutions obtained for rectangular or round rotor slots [6, 10]. The discrepancy lies in the fact that at small slip values, rotor leakage reactance and inductance in accordance with the exact formulas asymptotically approach certain boundary values. But, the dependencies presented in [13] do not have this property.

Research of induction motor drives is rather often performed using mathematical models available in Matlab SimPowerSystems. The virtual blocks of electric machines used make it possible to set values of the viscous friction coefficient, which allows reproducing motor nameplate data on models with high accuracy. But many researchers neglect this parameter, resulting in reduced accuracy of simulation [14, 15].

The feasibility of using adjustable-speed DC drive is dictated by the high power of the drydock main pumps and moderate average annual operation. The corresponding variable-frequency AC drives have a complex modular structure and much higher cost [16]. The payback period of frequency converters can significantly exceed a five-year term just by reducing energy consumption. Therefore, their application is inappropriate even given the high cost of DC motors and maintenance costs of the commutator. The lower cost is characteristic of soft starters of induction motors, but in case of their use the electric drive speed remains unadjustable in speed. Over the last decades, full-controlled power keys (IGBT) have become widespread in valve electric drives. Artificial commutation of such valves as part of active front ends allows minimizing a negative impact of electric drives on the network and regulating the reactive power. However, the corresponding voltage converters for the DC drive are similar in structure to the DC link frequency converters. They use a reverse pulse-width converter instead of a three-phase autonomous voltage inverter. In this regard, the cost of active front end drive is still rather high. In addition, the transistor power converter has a slightly lower efficiency compared to the thyristor one. This is explained by double energy conversion in the first and single in the second. Therefore, a complete thyristor drive, in particular Soviet-made KTEU series (up to 2,000 kW, from 1,000 to 12,000 kW), EKT (up to 2,000 kW), KTE (up to 1,000 kW), can be considered as the cheapest version of adjustable-speed drive of the main dock pumps. On the market you can find offers of such electric drives, which have long been in storage or out of service. However, it is known that, for example, KTE electric drives are still produced in an advanced version.

A great deal of scientific works is also devoted to the development and operation of a thyristor drive. Much of their focus is on the problems of synthesis and analysis of closed-loop control systems, improvement of dynamic and static characteristics of the drive, while the problems of interaction between the drive and the network fade into the background. When solving such problems, the electromechanical system is mostly considered separately, and the overall power system is formally replaced with an infinite-power supply [17]. However, it is known that negative effects of the thyristor converter with respect to the electrical network is distortion of voltage (at a considerable power of the electric drive) and current consumed [18]. In some cases, oscillation phenomena with frequencies different from the fundamental harmonic may occur, for example, if there is a capacitive load component in some electric consumers and resonance [19]. The analysis of behavior of a treed electric network with controlled rectifier and reactive load of both types requires knowledge of specific operating conditions of the basic elements of the system. Therefore, complex and unstable topology of the electric network complicates the system analysis of the drive, and the corresponding task may be not solved in general. Under these circumstances, the rationality of certain technical solutions can be checked by modeling the most probable and intense modes of joint operation of the drive and the network. For these reasons, a significant difference from other works is the detailed modeling of the electric network including large induction motors or thyristor drives. The mathematical model takes into account the finite power of the power source and capacity of the cable line. As noted in the literature, in particular [20], when determining the equivalent circuit parameters of the cable

line, capacity can be neglected if the line length is relatively small and the voltage does not exceed 20 kV. The results of a more detailed simulation suggest that such a statement is not unconditional. To increase energy performance, DC drives can be equipped with automatic harmonic filtering and reactive power control device, which requires the synthesis of a reactive power controller. These issues are given due attention in the work.

3. The aim and objectives of the study

The aim of the study is to prove the possibility of replacing unadjustable-speed AC drive of the drydock main pumps with adjustable-speed DC drive and to determine its structure taking into account the impact on the shipyard network.

To achieve this aim, the following objectives were set:

– to determine the viscous friction coefficient and T-shaped equivalent circuit parameters of a powerful deep-bar induction motor so that the catalog data are reproduced on a mathematical model with high accuracy;

– to create a mathematical model of the in-plant electric network in MATLAB SimPowerSystems and investigate the impact of unadjustable-speed AC drive of the drydock main pumps;

– to create a mathematical model of thyristor drives of the drydock main pumps and investigate their influence on the network considering or not the stray capacitance of the cable line;

– to investigate the effect of thyristor drives of the drydock main pumps on the network taking into account the stray capacitance of the cable line and in the presence of a capacitor bank;

– to create a mathematical model of automatic harmonic filtering and reactive power control device and investigate the effect of thyristor drives of the drydock main pumps on the network taking into account the stray capacitance of the cable line and in the presence of harmonic filtering and reactive power control device.

4. Materials and methods of studying the influence of the drydock main pumps drive on the electric network

The study of starting the main pump units was performed on a specific example of the drydock of the Okean shipyard, Mykolayiv. This choice is explained by the fact that this hydraulic facility has a design that is identical to the above, and the rated power of each of the four main electric pumps is 1,000 kW, i. e. large enough. The Mykolayiv drydock still remains one of the largest docks in Europe and has no analogues in the country to this day [1]. At the same time, due to the considerable operation period, the dock equipment increasingly requires repair or replacement, and obsolete technical systems are waiting for modernization.

4. 1. Determination of viscous friction coefficient and T-shaped equivalent circuit parameters of the AN16-41-12 induction motor

The drydock main horizontal centrifugal 48D-22 pumps of the Okean shipyard (Ukraine) are driven by large AN16-41-12 squirrel-cage induction motors with round-slot rotor [21]. There are also similar VAN16-41-12 vertical shaft motors, which, according to the specification indicated on the nameplate, differ slightly from the horizontal implementation, but are described in more detail in the literature [5]. According to the classification [13], such motors belong to the third group, that is, they are characterized by significant displacement of the rotor current, but the saturation of the tooth area can be neglected. According to [13], motor parameters can be considered invariable when the rotor slip becomes close to or less than the critical value. The parameters of the equivalent circuit must ultimately be specified in the induction motor block in MATLAB SimPowerSystems, which does not take into account the power loss in the stator and rotor steel. Therefore, the T-shaped equivalent circuit should have a magnetizing branch with pure inductance. In order to maintain the model and motor equivalence in terms of rated power, it is advisable to consider power losses, i. e. mechanical and in steel, by the coefficient of viscous friction. Determination of equivalent circuit parameters is carried out in three stages. First, we find the values of equivalent circuit parameters that correspond to the sub-critical values of motor slip. Then we find the values of the parameters that are achieved in the short-circuit mode of the machine. After that, we approximate the rotor resistance by elementary functions that are asymptotic at a small absolute value of slip. Note that during the first stage of calculation, for the sake of precision, it is necessary to abandon approximate computation of the critical slip by the simplified Kloss formula. So, we find the electromagnetic torque of the motor by the known values of useful power P_{nom}, angular speed ω_{nom} and efficiency η_{nom} for the rated mode:

$$M_{enom} = \frac{P_{nom}}{\omega_{nom}}\left(1+\beta_{nom}\frac{1-\eta_{nom}}{\eta_{nom}}\right), \quad (1)$$

where β_{nom} is the ratio of constant and total power losses in the rated mode. During the calculations, $\beta_{nom}=0.49$ was taken [22]. Thus, constant and variable power losses in the rated mode are almost the same and the rated efficiency is close to the maximum that occurs at the motor load factor $\alpha_{\max} \approx \sqrt{\beta_{nom}/(1-\beta_{nom})} \approx 0.98$. Note that if $\beta_{nom}=0.32886$, the maximum efficiency would correspond to the load factor $\alpha_{\max}\approx 0.7$.

The stator active resistance is found by the formula:

$$R_s = \frac{1}{3I_{snom}^2}\left(\frac{P_{nom}}{\eta_{nom}} - M_{enom}\omega_1\right), \quad (2)$$

where I_{snom} is the rated stator phase current,

$$\omega_1 = 2\pi f_s / p \quad (3)$$

– angular speed of the stator magnetic field, f_s – network frequency, p – number of pole pairs.

The reduced rotor active resistance is calculated:

$$R'_{r0} = \frac{s_{nom}}{C_1}\left(R_i - R_s + \sqrt{R_i\left(1-\frac{1}{k_m}\right)\left(R_i\left(1+\frac{1}{k_m}\right)-2R_s\right)}\right), \quad (4)$$

where

$$R_i = 3U_{nom}^2 / \left(2C_1\omega_1 M_{enom}\right) \quad (5)$$

– imaginary active resistance, on which at the rated operating stator phase voltage U_{nom}, approximately double the

rated value of the electromagnetic power of the induction motor is dissipated;

$$s_{nom} = (\omega_1 - \omega_{nom}) / \omega_1 \quad (6)$$

– rated slip;

$$C_1 = \left|1 + (R_s + jX_s) / (jX_m)\right| \quad (7)$$

– coefficient of reduction of the T-shaped equivalent circuit parameters to the L-shaped circuit (stator leakage), the initial value of which is taken as a unit, X_s, X_m is the leakage inductance of the stator winding and magnetizing branch, k_m is the maximum torque ratio. It should be clarified that the maximum torque ratio of the induction motor means the ratio of the critical shaft torque to the rated shaft torque. However, due to the small discrepancy between the electromagnetic and mechanical torque values, the ratio is often calculated using the electromagnetic torque values [23]. Since in the proposed model mechanical power losses are increased by the value of losses in steel and additional, it is necessary to calculate the corrected value of the maximum electromagnetic torque ratio:

$$k_m = (\lambda_m P_{nom} / \omega_{nom} + b\omega_{nom}) / M_{enom}, \quad (8)$$

where λ_m is the reference value of the maximum shaft torque ratio;

$$b = \frac{\beta_{nom} P_{nom}}{\omega_{nom}^2} \frac{1 - \eta_{nom}}{\eta_{nom}} \quad (9)$$

– coefficient of viscous friction. It should be noted that in the formula (8), the viscous friction torque is calculated approximately by the rated speed value instead of the critical one, but this does not lead to a significant error.

Stator and rotor leakage inductances are assumed to be equal and calculated as follows:

$$X_s = X'_{r0} = \frac{1}{1 + C_1} \sqrt{\left(\frac{R_i}{k_m} - 2R_s\right) \frac{R_i}{k_m}}. \quad (10)$$

Now let's determine the rated current, impedance and terminal voltage of the operating loop:

$$I'_{rnom} = \sqrt{M_{enom} \omega_1 s_{nom} / (3R'_{r0})}, \quad (11)$$

$$Z'_{rnom} = \sqrt{(R'_{r0} / s_{nom})^2 + X'^2_{r0}}, \quad (12)$$

$$U_{0nom} = Z'_{rnom} I'_{rnom}. \quad (13)$$

The rated power factor is:

$$\cos\varphi_{nom} = P_{nom} / (3\eta_{nom} U_{nom} I_{snom}). \quad (14)$$

If the input data include all the values in the equation (14), further calculations should be made using the estimated power factor value. It is advisable to first compare this value with the reference to check the accuracy of the calculations and consistency of the original data.

The rated magnetizing current is determined according to the expression:

$$I_{0nom} = I_{snom} \frac{Z_{inom}}{Z'_{rnom}} \times$$

$$\times \sqrt{1 - \frac{2U_{nom} \cos(\varphi_{inom} - \varphi_{nom})}{U_{inom}} + \left(\frac{U_{nom}}{U_{inom}}\right)^2}, \quad (15)$$

where

$$U_{inom} = Z_{inom} I_{snom} \quad (16)$$

– resistive voltage drop Z_{inom} caused by the flow of stator rated current, and

$$Z_{inom} = \sqrt{(R'_{r0} / s_{nom} + R_s)^2 + (X_s + X'_{r0})^2}, \quad (17)$$

$$\varphi_{inom} = \text{arctg}\{(X_s + X'_{r0}) / (R'_{r0} / s_{nom} + R_s)\} \quad (18)$$

– modulus and angle of the imaginary equivalent resistance of the T-shaped equivalent circuit, which would take place in the event of magnetizing branch fault; φ_{nom} – rated phase shift between the motor stator voltage and current. It should be noted that the equivalent impedance, which is determined by formulas (17) and (18), has an operating loop of the simplified L-shaped equivalent circuit of the induction motor at the rated slip.

The magnetizing branch resistance is determined on the basis of (13) and (15), after which it is possible to calculate a new, more accurate value of the coefficient:

$$C_1(2) = 1 + X_s(1) / X_m(1), \quad (19)$$

and, if necessary, repeat the calculation of parameters. The iterative process has rapid convergence, usually the number of iterations to achieve the desired accuracy:

$$\Delta C_1(N) = \left|C_1(N+1) - C_1(N)\right|, \quad (20)$$

does not exceed 4–5. However, despite the high accuracy of determining the stator leakage factor, the original data can be reproduced in the mathematical model only with some error since the calculation is based on approximate formulas (4), (10). For the same reason, there is a discrepancy between the values of voltage across the magnetizing resistance U_{0nom}, if the value is calculated in different ways. The first is to use the formula (13) and the second is based on the formula:

$$U_{0nom} = \sqrt{U_{nom}^2 - 2U_{nom} Z_s I_{snom} \cos(\varphi_s - \varphi_{nom}) + Z_s^2 I_{snom}^2}, \quad (21)$$

where

$$Z_s = \sqrt{R_s^2 + X_s^2}, \quad (22)$$

$$\varphi_s = \text{arctg}\{X_s / R_s\} \quad (23)$$

– modulus and angle of the stator impedance. Generally speaking, the parameters of the equivalent circuit can be searched using equation (21) instead of (13). Then the need to use the equations (11), (12) disappears, but there is a discrepancy in the value of reduced rotor current. The results of the calculations differ in both cases, but insignificantly.

As the analysis shows, the parameters of the equivalent circuit can be determined in such a way that only the value of critical electromagnetic torque ratio will be characterized by a small error. For this, the stator leakage inductance can be found as the root of the quadratic equation:

$$a_0 X_s^2 + a_1 X_s + a_2 = 0, \tag{24}$$

the coefficients of which are

$$a_0 = 1 - k_{inom}^2 / C_1^2, \tag{25}$$

$$a_1 = 2\left(k_{inom}^2 X_{\Sigma L} / C_1^2 - Z_b \sin\varphi_{nom}\right), \tag{26}$$

$$a_2 = Z_b^2 + R_1^2 - k_{inom}^2 \left(\frac{X_{\Sigma L}^2}{C_1^2} + \frac{R_{r0}'^2}{s_{nom}^2} \right) - 2 Z_b R_1 \cos\varphi_{nom}, \tag{27}$$

where

$$k_{inom} = I'_{rnom} / I_{snom} \tag{28}$$

– rated current ratio of the operating loop of the T-shaped equivalent circuit;

$$Z_b = U_{nom} / I_{snom} \tag{29}$$

– base resistance;

$$X_{\Sigma L} = \sqrt{\left(R_i / k_m - 2R_s\right) R_i / k_m} \tag{30}$$

– total reactance of the operating loop of the specified L-shaped equivalent circuit. Then the reduced rotor leakage inductance is found as follows:

$$X'_{r0} = \left(X_{\Sigma L} - X_s\right) / C_1, \tag{31}$$

It is also possible that the stator leakage inductance is determined, as before, by the formula (10), but the rotor leakage inductance is found using equations (21), (11)–(13). In this case, for $X'_{r0} \neq X_s$, the equation (30) turns into inequality. In both cases, the leakage factor cannot be found by the fixed-point iteration method. This factor can be determined by the above method – in advance, or if the desired critical electromagnetic torque ratio is reached. The leakage factor can also be found provided that the leakage inductance of the stator and reduced – of the rotor are equal in the process of their joint calculation.

Let us now proceed to determining the values of the equivalent circuit parameters in the short-circuit mode. This mode is characterized by a certain increase in the reduced rotor active resistance compared to the value R'_{r0} and a decrease in the reduced leakage inductance compared to X'_{r0}, other parameters remain unchanged. Find the value of the power factor that is achieved in the short-circuit mode:

$$\cos\varphi_1 = \left(3k_i^2 I_{snom}^2 R_s + k_{m1} M_{enom} \omega_1\right) / \left(3U_{nom} k_i I_{snom}\right), \tag{32}$$

where k_i, k_{m1} is the initial starting current and torque ratio. The latter value should be specified using the formula that includes the reference value of the initial starting torque ratio λ_{m1}:

$$k_{m1} = \lambda_{m1} P_{nom} / \left(\omega_{nom} M_{enom}\right). \tag{33}$$

The imaginary current of the magnetizing branch I_{0i} that would occur in the case of applying the voltage U_{nom} to its terminals, as well as the stator impedance drop U_{s1} caused by the flow of short-circuit current $k_i I_{snom}$ is

$$I_{0i} = U_{nom} / X_m, \tag{34}$$

$$U_{s1} = Z_s k_i I_{snom}. \tag{35}$$

The active, reactive components and total short-circuit current of the operating loop are determined by the formulas:

$$I'_{r1a} = \left[k_s \sin\left(\varphi_s - \varphi_1\right) + \cos\varphi_1\right] k_i I_{snom}, \tag{36}$$

$$I'_{r1x} = I_{0i} - \left[k_s \cos\left(\varphi_s - \varphi_1\right) + \sin\varphi_1\right] k_i I_{snom}, \tag{37}$$

$$I'_{r1} = \sqrt{I'^2_{r1a} + I'^2_{r1x}}, \tag{38}$$

where φ_1 is the phase shift between the rated voltage and short-circuit current, and

$$k_s = Z_s / X_m \tag{39}$$

– relative value.

Using the results obtained, we find the reduced active, total and reactive resistance of the rotor in the short-circuit mode:

$$R'_{r1} = k_{m1} M_{enom} \omega_1 / \left(3I'^2_{r1}\right), \tag{40}$$

$$Z'_{r1} = \frac{U_{nom}}{I'_{r1}} \sqrt{1 - \frac{2U_{s1}\cos\left(\varphi_s - \varphi_1\right)}{U_{nom}} + \left(\frac{U_{s1}}{U_{nom}}\right)^2}, \tag{41}$$

$$X'_{r1} = \sqrt{Z'^2_{r1} - R'^2_{r1}}. \tag{42}$$

The approximating rotor resistance functions $R'_r = R'_r(s)$ and $X'_r = X'_r(s)$ must satisfy the conditions:

$$\lim_{s\to 0} R'_r(s) = R'_{r0}, \quad R'_r(s_c) \approx R'_{r0}, \quad R'_r(1) = R'_{r1}, \tag{43}$$

$$\lim_{s\to 0} X'_r(s) = X'_{r0}, \quad X'_r(s_c) \approx X'_{r0}, \quad X'_r(1) = X'_{r1}. \tag{44}$$

Given these conditions, the following formulas are proposed:

$$R'_r(s) = R'_{r0} + \left(R'_{r1} - R'_{r0}\right) e^{k_r (s-1)/s}, \tag{45}$$

$$X'_r(s) = X'_{r1} + \left(X'_{r0} - X'_{r1}\right)\left(1 - e^{k_x (s-1)/s}\right), \tag{46}$$

where k_r, k_x are some coefficients taken to be equal to $k_r = k_x = 0.5$. Formulas (45), (46) are essentially the same, as can be seen if you remove the brackets in the expression $X'_r(s)$, but the advantage of this form is the positivity of variable components of resistance. Though the motor in question is squirrel-cage type, its model can be created using the wound-rotor induction motor block. In this case, the intrinsic active resistance and leakage inductance of the motor are set to be equal to R'_{r0} and $L'_r = X'_{r1} / \left(2\pi f_s\right)$. As the external resistance, the alternate active-inductive circuits are

used, which are connected in wye and described by the same equations. For the «A» phase, we have:

$$L'_{rvar}(s)\frac{di'_{ra}}{dt}+\left(\frac{dL'_{rvar}}{ds}\frac{ds}{dt}+R'_{rvar}(s)\right)i'_{ra}=u'_{ra}, \quad (47)$$

where

$$L'_{rvar}=\frac{X'_{r0}-X'_{r1}}{2\pi f_s}\left(1-e^{k_x(s-1)/s}\right) \quad (48)$$

– external variable inductance,

$$R'_{rvar}=\left(R'_{r1}-R'_{r0}\right)e^{k_r(s-1)/s} \quad (49)$$

– external variable active resistance. The first term in the brackets of the left part of the equation (47) can be considered as a transient component of active resistance caused by the dependence of the rotor leakage flux linkage on the rotor current frequency due to its displacement. We calculate the derivative of inductance by slip and its value at characteristic points:

$$\frac{dL'_{rvar}}{ds}=-\frac{X'_{r0}-X'_{r1}}{2\pi f_s}\frac{e^{k_x}}{k_x}\left(\frac{k_x}{s}\right)^2 e^{-\frac{k_x}{s}}, \quad (50)$$

$$\lim_{s\to 0}\frac{dL'_{rvar}}{ds}=0,\ \left.\frac{dL'_{rvar}}{ds}\right|_{s=1}=-k_x\frac{X'_{r0}-X'_{r1}}{2\pi f_s}. \quad (51)$$

Find the second derivative of inductance:

$$\frac{d^2L'_{rvar}}{ds^2}=\frac{X'_{r0}-X'_{r1}}{2\pi f_s}\frac{e^{k_x}}{k_x}\left(\frac{2k_x}{s}-\left(\frac{k_x}{s}\right)^2\right)e^{-\frac{k_x}{s}}\frac{k_x}{s^2}. \quad (52)$$

Zero of the second derivative $s=k_x/2$ is obvious, at which the first derivative reaches its minimum value:

$$\left.\frac{dL'_{rvar}}{ds}\right|_{s=k_x/2}=-\frac{4e^{k_x-2}}{k_x}\frac{X'_{r0}-X'_{r1}}{2\pi f_s}. \quad (53)$$

The largest value of the modulus derivative dL'_{rvar}/ds on the segment $s\in[0;1]$ is rather small, and the slip during the transient process changes rather slowly, $|ds/dt|<0.5\ s^{-1}$. In view of this, it is possible to neglect the first term in the brackets of the left part of the equation (47) compared to the value R'_{rvar} and simplify this equation. Then we have:

$$L'_{rvar}(s)\frac{di'_{ra}}{dt}+R'_{rvar}(s)i'_{ra}=u'_{ra}. \quad (54)$$

Following the above calculation procedure, it was succeeded to find the required values of the viscous friction coefficient and T-shaped replacement circuit parameters of the induction motor, which provide high accuracy of the mathematical model. The results of the calculations are presented in Table 1, and motor static characteristics – in Fig. 1.

In the calculations, $k_{m1}=\lambda_{m1}$ and $k_m=\lambda_m$ are taken since formulas (8) and (33) were obtained after the bulk of the calculations had been completed. However, the discrepancy between the real motor and its mathematical model, which is the result of increased initial starting and maximum electromagnetic torque ratio, is acceptable. The motor model is more sophisticated in terms of electromechanical energy conversion in static and dynamic modes. In particular, the motor model is characterized by shorter start-up time, all things being equal. To estimate the maximum electromagnetic torque ratio of the mathematical model of the induction motor, a virtual load with a static speed-torque characteristic was created, described by the equation:

$$M=k_m M_{enom}\left(n/n_v\right)^{10}-\pi bn/30, \quad (55)$$

where n_v=475; 477.5; 480 rpm. Equation (55) ensures stable operation of the induction motor model in the vicinity of the critical point of its speed-torque characteristic, in contrast to the steady static moment. Fig. 1 shows the curves plotted according to equation (55), but without the linear component of the moment, for the extreme speed values n_1 and n_3. The static characteristics of the induction motor are based on the refined L-shaped equivalent circuit. The electric speed-torque characteristic establishes the relationship between the relative value of the angular speed of the rotor and the current of the operating loop of the T-shaped circuit, and the speed-torque characteristic reflects the relationship between the relative value of the angular speed and the electromagnetic moment. As can be seen from Fig. 1, the desired nature of changes in rotor resistance, expressed in relative units, is achieved, and within the operating branch of the motor speed-torque characteristic, the rotor parameters are almost constant.

Table 1

Results of determining the AN16-41-12 motor parameters

Parameter	Value	
T-shaped equivalent circuit	Idling	Short circuit
R'_s, Ohm	0.62223	0.62223
X_s, Ohm	3.3549	3.3549
X_m, Ohm	79.884	79.884
R'_r, Ohm	0.28976	0.75622
X'_r, Ohm	3.3549	1.9152
Motor	Specified (corrected)	Estimated
b, Nms/rad	–	13.515
P_{nom}, kW	1,000	1000.1
U_{nom}, V	6,000	6000
I_{snom}, A	121	120.99
n_{nom}, rpm	495	495.01
$\cos\varphi_{nom}$	0.85 (0.85419)	0.85422
η_{nom}	0.931	0.93113
I_{s1}/I_{snom}	5.3	5.3
M_{e1}/M_{enom}	0.85 (0.82021)	0.85
M_{emax}/M_{enom}	2.2 (2.1579)	2.1983, when ω_3=479.963 rad/s 2.2063, when ω_2=477.636 rad/s 2.1863, when ω_1=474.704 rad/s

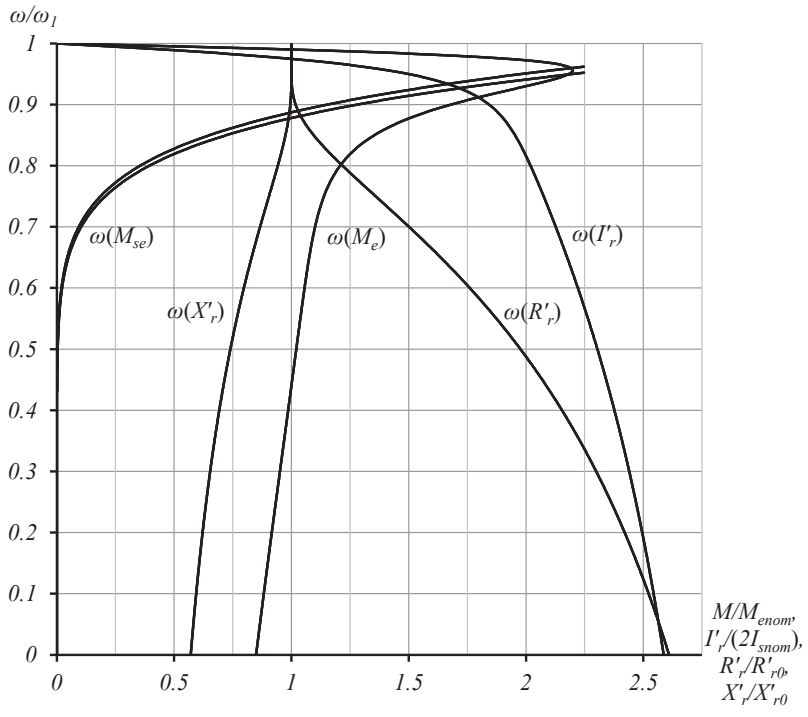

Fig. 1. Static characteristics of the AN16-41-12 motor

load, which is connected in parallel with the main pump motors, consumes an active power of 250 kW at a rated line voltage of 6 kW. The power factor is 0.8, the phase resistances are wye-connected. Similarly, the load block is configured that models the electric equipment connected at the node of the cable line sections. The number of AN16-41-12 motors, the parallel operation of which is provided in the mathematical model, is three, and the fourth electric pump unit is considered as spare. It is known that in order to reduce the load on the electric network, the motors of the main centrifugal pumps are started alternately against a closed discharge valve of pressure lines. Therefore, starting of the last third electric pump unit when the other two are already in operation or continue to operate against a closed discharge valve has the most significant impact on the electric network. For this reason, in the mathematical model, the static load of all three motors is the same, has a fan character and corresponds to dry running of 48D-22 pumps. The operating mode under study is starting of the last electric pump unit against a closed discharge valve while dry running of the first two.

4. 2. Study of the influence of AC drive on the network

To evaluate the influence of starting currents of AN16-41-12 squirrel-cage induction motors of the main pump units of the docking pump station on the network, a mathematical model was created in MATLAB SimPowerSystems, the block diagram of which is shown in Fig. 2.

The TDNS-10000/35 three-phase transformer, having a higher line voltage of 35 kV, lower 6 kV, rated at a total power of 10,000 kVA, acts as the finite-power source of the network. The transformer allows on-load tap changing within ±12 % [24]. In the mathematical model of the transformer, the tap changer function is not implemented, but the U/D-11 windings group is taken into account. The transformer is powered by rated voltage from an ideal AC voltage source, phase emf of which are connected in wye. In turn, the main pump motors receive electric energy from the main transformer via the cable line consisting of two sections, at the beginning and at the end of each of which the parallel-connected electric consumers are switched on. The cable line uses a tight-core aluminum cable. The first section of the line is double, has a length of 1.6 km and a cross section of 3×150 mm^2, and the second section is single, has a length of 0.9 km and a cross section of 3×185 mm^2. Given the length and number of parallel branches, each section of the cable line is modeled using three Pi Section Line blocks, one per phase. In all Pi Section Line blocks, the cable line equivalent circuit in the form of a single pi-section, whose resistance is calculated by the specific parameters of the cable line phase, is used [20, 24]. The boiler house, as a consumer of electric energy, is described by the active-inductive load, which is connected in wye to the terminals of the transformer secondary winding. The active power of the boiler house is 2 MW at a rated line voltage of 6 kV, power factor of 0.8. The main pumps usually operate together with a pair of drainage pumps and one large stripping pump, which removes the water coming into the pit from the cementation patterns of the drydock chamber. Taking into account the power of these pumps, the equivalent active-inductive

The joint inertia of each pump unit is defined as equal to twice the rotor moment of inertia, taking into account the mass of the pump impeller and the added mass of water, which filled its channels. Assuming insignificant speed variations and, as a consequence, practical constancy of the rotor parameters of the first pair of motors during the start-up of the third one, these motors are considered in the simulation as squirrel-cage type, with the initial slip value close to zero. This approach significantly reduces the calculation time of transients. The started motor is represented in the mathematical model of the electric network using the block of wound-rotor induction machine, to which external variable active-inductive resistance is connected. The active resistance and inductance are calculated in the angular speed function with the help of Subsystem shown in Fig. 2, *b*. The restriction block serves to eliminate the error of dividing the slip value by zero in the blocks using formulas (40), (41). The instant voltage drop across the external variable resistance phases is calculated using Subsystem1-3, the block diagram of which is shown in Fig. 2, *c*. The graphs of the transients for the relative stator current, relative electromagnetic torque and absolute speed of the pair of squirrel-cage motors are identical (Fig. 3, *a*). The wound-rotor induction motor corresponds to Fig. 3, *b*.

At the initial moment of time, the pair of squirrel-cage motors rotate at a speed close to synchronous, and the static load is absent, so a short transient occurs as a result of applying the supply voltage to the stator winding terminals. After a 1 s period of time, the motors already have a practically steady speed, but static torque surge occurs and the transient begins again. Within the next second, the transient of perturbation of the squirrel-cage motors almost comes to an end, and at the 3 s timepoint, the induction motor with the wound rotor, which was static up to that moment, is connected to the network. Starting of the wound-rotor induction motor, which formally replaced the AN16-41-12 squirrel-cage motor with variable parameters, lasts about 8.5 s and is accompanied by a significant decrease in the supply voltage, as evidenced by the graph in Fig. 4.

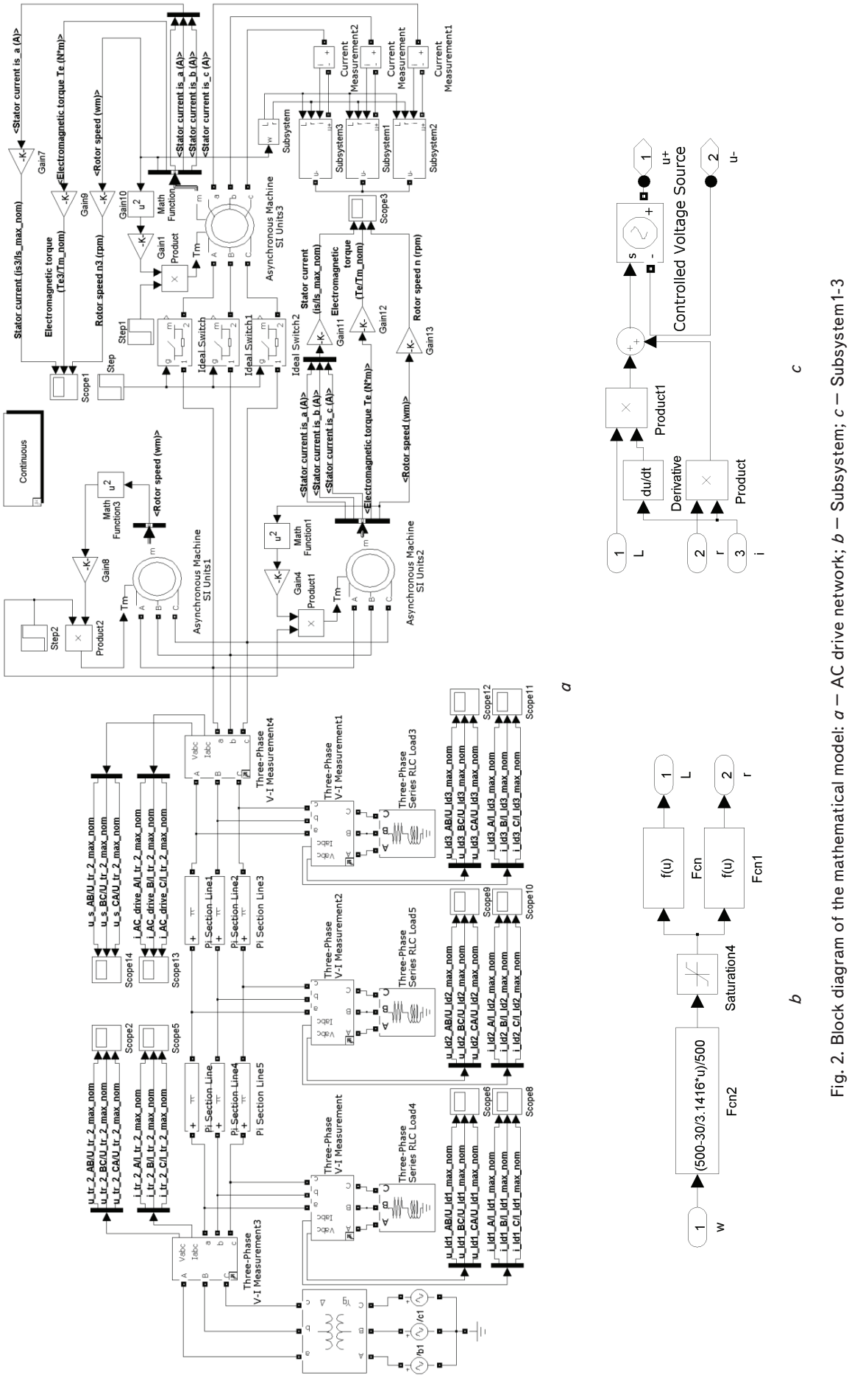

Fig. 2. Block diagram of the mathematical model: *a* – AC drive network; *b* – Subsystem; *c* – Subsystem1-3

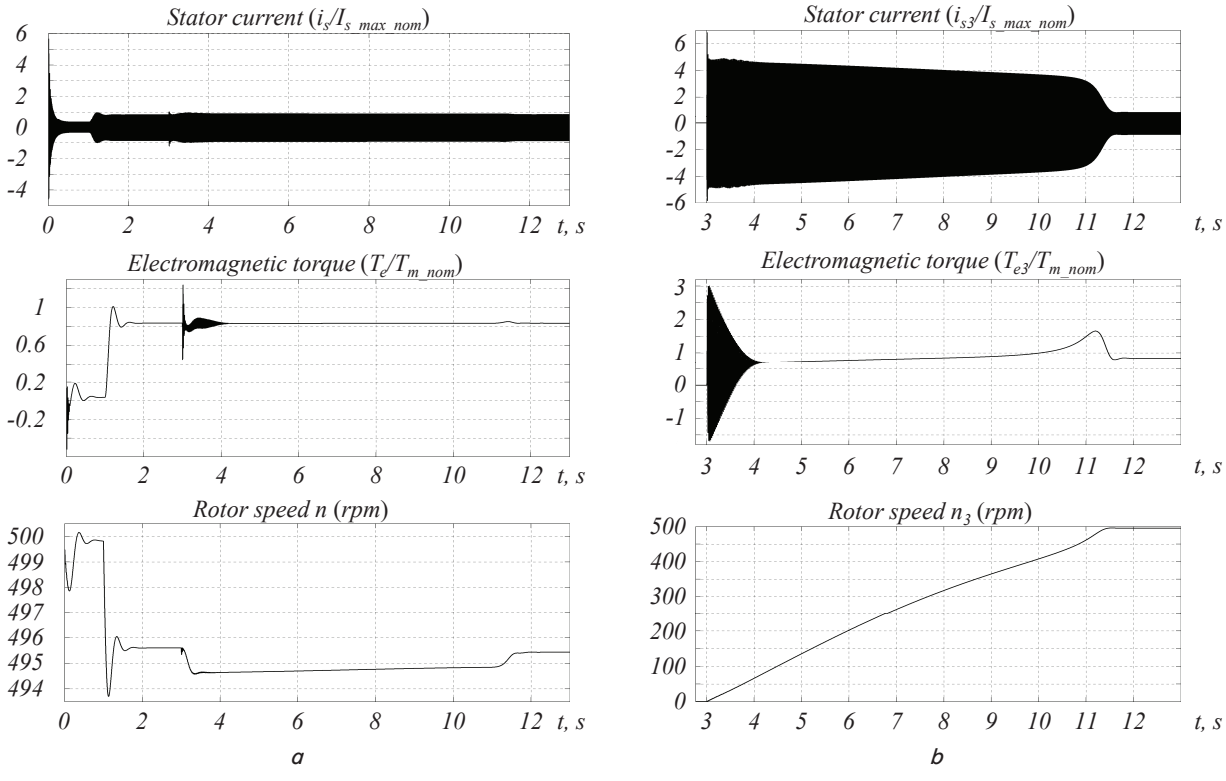

Fig. 3. Graphs of transients of the induction motor: *a* — squirrel-cage; *b* — wound-rotor

The relative deviation of the stator voltage during motor start-up is about 11...13 %. As can be seen from Fig. 3, *a*, the drop in the supply voltage causes a corresponding small decrease in the speed of the pair of squirrel-cage motors, which is explained by the high rigidity of their speed-torque characteristics. At the end of the first section of the cable line, the voltage deviation during the transient is approximately 8...10 % and 6...7 % at the main transformer output.

During the motor start-up, the current load of the main transformer is close to the rated one, as evidenced by the graph shown in Fig. 5.

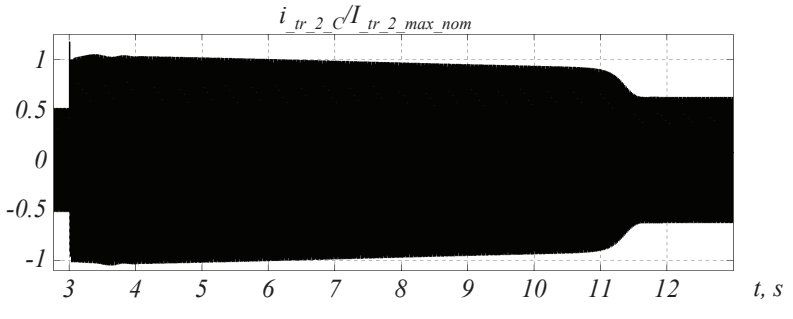

Fig. 5. Graph of the transient of the secondary line current of the main transformer

In comparison with the transient one, the quasi-steady value of instantaneous current decreases accordingly, but increases with respect to the quasi-static mode of only two electric pump units.

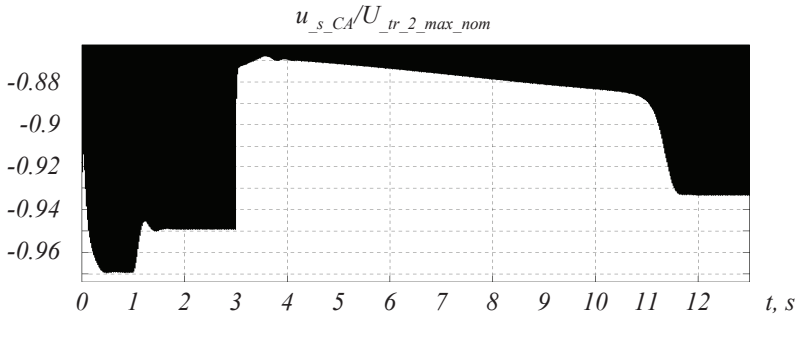

Fig. 4. Graph of the transient of the stator line voltage

4. 3. Study of the influence of DC drive on the network

For starting each of the four 48D-22 pumps, the Soviet-made MPE-1000-630 UKHL3 DC motor, designed to drive the traction and lift mechanisms of large walking excavators, for example, ESh20-90, was selected [25, 26]. The selected motor has independent ventilation and is designed for long-term operation with reduced speed at rated load. To reduce the area of intermittent current and limit the ripples, the Soviet-made SROSZ-2000MUKHL4 reactor was included in the armature coil of the motor [27]. The Soviet TSZP-1600/10U3-1 dry transformer is used to coordinate the network voltage and motor power supply, as well as to limit the current growth rate of controlled rectifier thyristors [27]. Thus, each electric pump unit receives power from its transformer. Generally speaking, the number of transformers may be less than four, if

their rated power is increased, but the parallel connection of several thyristor converters to a single transformer may require additional current limiting reactors. This option is not considered in this paper. The voltage converter has a three-phase bridge circuit, rated output voltage of 460 V, rated half-period average current of 2,500 A. The motor is powered by the converter with a voltage that is lower than the rated supply voltage of the armature coil (600 V). This provides the operating mode of the 48D-22 pump close to the rated one, because the rated value of motor speed and power is greater compared to the pump. The pulse-phase control system has a control characteristic of the arccosine type, whereby the resulting control characteristic of the converter acquires a linear form. For limiting the armature current in dynamic modes and precise speed control during operation, the DC drive has a double-circuit automatic control system with subordinate coordinate regulation [28]. The current circuit is set to the modular optimum and the speed – to the symmetric optimum. Given this, both circuit controllers are synthesized as proportional-integral. As is known, the gain of the current controller depends on the parameters of the armature coil and the parameters of the finite-power AC voltage source reduced to it and, in particular, on switching resistance. Thus, the current controller parameters were determined taking into account the leakage inductance and active resistance of the TSZP-1600/10U3-1 transformer, but the influence of the network was neglected. The block diagram of the mathematical model of the network in the SimPowerSysytems environment with DC drives of the main pumps is presented in Fig. 6, *a*.

It includes the subsystems of the first and second level, which are shown, respectively, in Fig. 6, *b*, 7, *a*, 8. This block diagram is generally similar to that shown in Fig. 2, *a*. But this one, instead of three blocks of induction motors, contains four DC Drive1-4 subsystems of thyristor drive with the fan-type load that corresponds to dry running of 48D-22 centrifugal pumps. Unlike induction, DC motor loads are artificially increased (750 kW and 900 kW at 485 rpm, respectively) to control the operating mode of the system, which is quite close to rated. In addition to the fan component of the static torque, the reactive torque of $10M_{enom}$ is applied to each motor shaft, except for the fourth one, at certain intervals for their rapid deceleration. Only one of the pump units is equipped with the automatic control system, the block diagram of which is shown in Fig. 6, *b*, and the other three have an open loop drive and are controlled by a common signal. The automatic control system limits the starting current of each motor to $1.2I_{nom}$. To reduce the calculation time, the thyristors are modeled as ideal switches, which in the open state are characterized by a constant voltage drop value of 1.5 V. Therefore, for the inviolability of the first law of commutation, the three-phase active-capacitive load is connected in wye at the converter input. The value of active and reactive power is, respectively, 10 W and 20 VAr at a line voltage of 410 V. At the converter output, the resistor with active resistance of 10 kOhm is included. The Voltmeters subsystem measures the line voltages at the converter input, which are used as input signals of the synchronized 6-pulse generator. Because of the commutation phenomenon, corresponding short-term bursts appear in the timing diagrams of the secondary line voltages and, as a result, the correct operation of the synchronized 6-pulse generator may be disrupted. To prevent errors in the switch control process, this subsystem contains a resonance filter tuned to the network frequency [29]. The block diagram of the Voltmeters subsystem is presented in Fig. 8, *a*, the active resistance of the filter is 10 kOhm, the value of inductance and capacitance is assumed to be identical, equal to $1/(2\pi f_s)$. All DC drives are connected to the network in parallel with the components of harmonic filtering and reactive power control device. Its model is presented in the form of the Harmonic Filters & Reactive Power Control subsystem, the block diagram of which is shown in Fig. 7, *a*.

In general, the harmonic filtering and reactive power control device includes such components as a capacitor bank, double tuned three-phase harmonic filter and adjustable reactor. The rated reactive power of the capacitor bank is 7,200 kVAr. The filter is tuned to the fifth and seventh current harmonics, the phases are connected in delta. The rated reactive power of the filter is 1,500 kVAr and the q-factor is 64. According to these data, the values of inductance, capacitance and active resistance of the filter phases can be obtained using the Generate Report/Generate the circuit netlist report commands in the powergui block or the following formulas:

$$L_1 = \frac{\gamma k_1 k_2 - 1}{\left(k_1^2 - 1\right)\left(k_2^2 - 1\right)} \frac{1}{\Omega_{nom}} \frac{3U_{nom}^2}{Q_{nom}}, \tag{56}$$

$$C_1 = \frac{\gamma}{k_1 k_2} \frac{1}{\Omega_{nom}^2 L_1}, \tag{57}$$

$$C_2 = \frac{\gamma}{\left(\gamma k_2 - k_1\right)\left(k_2 - \gamma k_1\right)} \frac{1}{\Omega_{nom}^2 L_1}, \tag{58}$$

$$L_2 = \frac{1}{\gamma k_1 k_2} \frac{1}{\Omega_{nom}^2 C_2}, \tag{59}$$

$$R_2 = qL_2\Omega_{nom}\sqrt{\gamma k_1 k_2}, \tag{60}$$

where k_1, k_2 are the ordinal numbers of harmonics, Ω_{nom}, U_{nom}, Q_{nom} are the rated values of circular frequency, phase voltage and total reactive power; q is the q-factor; γ is some coefficient, which, for $k_1=5$, $k_2=7$, takes the value of $\gamma=0.942858$. It can be shown that with such filter tuning, when $R_2\to\infty$ and $\gamma=1$, the boundary equality always holds:

$$\frac{dX_f(\Omega)/d\Omega\big|_{\Omega=k_1\Omega_{nom}}}{dX_f(\Omega)/d\Omega\big|_{\Omega=k_2\Omega_{nom}}} = \frac{k_2}{k_1}, \tag{61}$$

where X_f is the equivalent phase resistance of the filter at an arbitrary frequency Ω.

The reactor power automatically changes depending on the value of reactive power consumed by the simultaneously operating DC drives. As a result, the total reactive power consumed by the TSZP-1600/10U3-1 loaded transformers together with the harmonic filtering and reactive power control device is within permissible limits. The maximum reactor power is determined by the sum of the rated power of the capacitor bank and the filter. The excess power reactor is described by the Three Phase Dynamic Load block, which is controlled by a single-circuit automatic control system by the deviation of the total reactive power. The initial operating conditions of the Three Phase Dynamic Load block are most conveniently determined using the Machine Initialization tool in the powergui block.

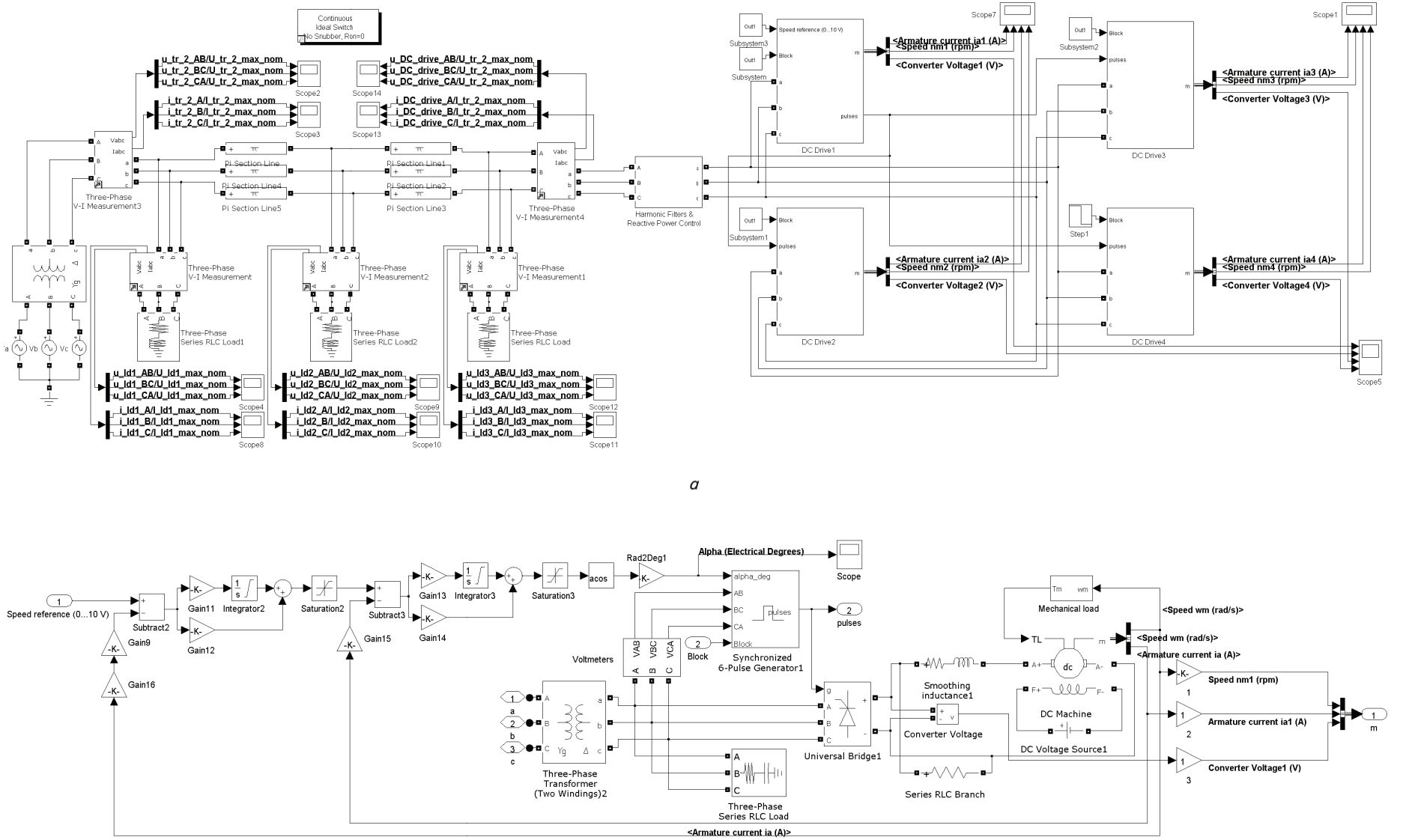

a

b

Fig. 6. Block diagram of the mathematical model: *a* — DC drive network; *b* — DC Drive1 subsystem

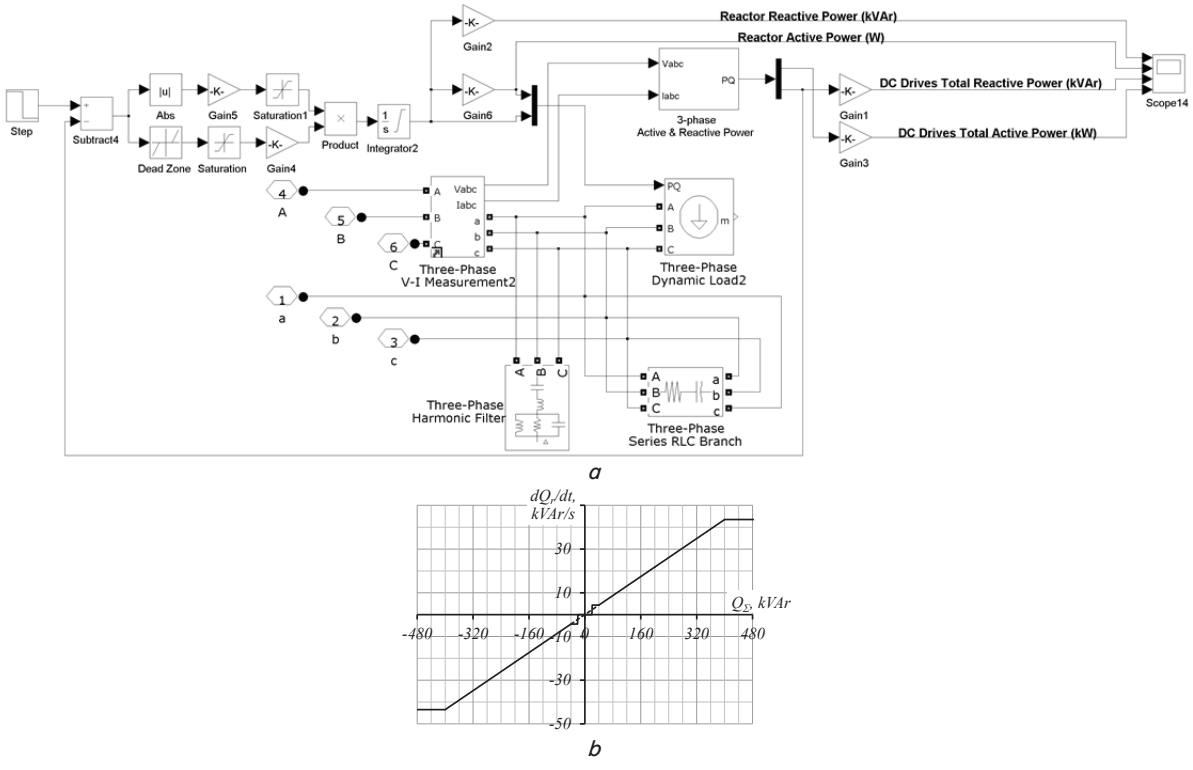

a

b

Fig. 7. Model of the harmonic filtering and reactive power control device:
a — block diagram of the Harmonic Filters & Reactive Power Control subsystem;
b — graph of the input signal of the integrating link against error

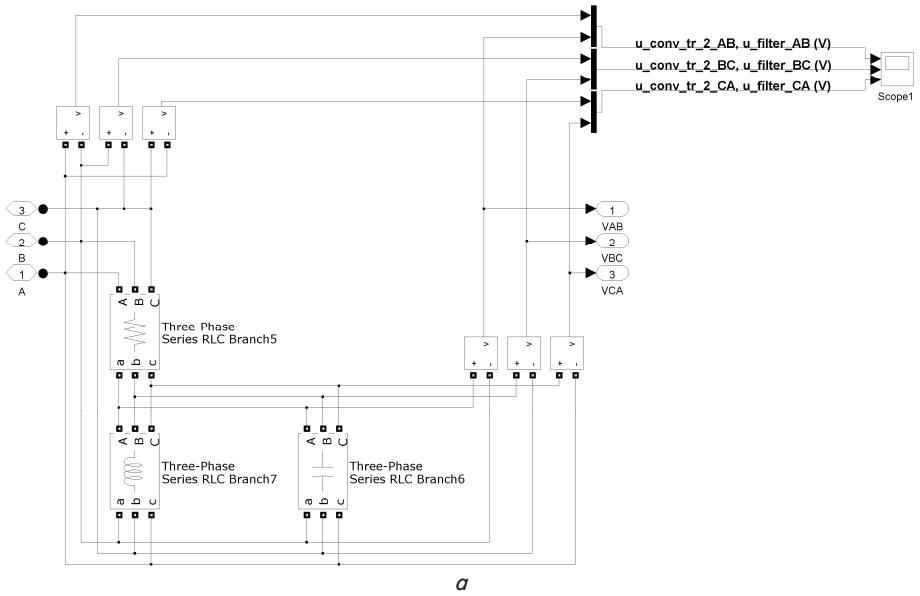

a

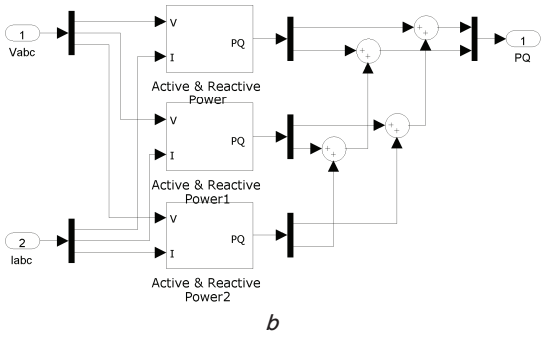

b

Fig. 8. Block diagram of the second level subsystem:
a — Voltmeters; *b* — 3-phase Active & Reactive Power

Acceptable transient quality and desired level of accuracy in steady-state conditions are ensured by the use of an integrated variable gain reactor power controller. The rate of changes in the reactor power depends in some way on the error of total reactive power control. The corresponding graph is shown in Fig. 7, *b*. It shows that the controller, among other things, performs the function of limiting the rate of changes in the reactor power at a given level, and the accuracy of total reactive power control is determined by the gap – 20...20 kVAr. Fig. 8, *b* shows the subsystem designed to calculate the total active and reactive power consumed by DC drives from the network, taking into account the harmonic filtering and reactive power control device. The subsystem under consideration works correctly even when the three-phase voltage and current system is unbalanced. The last difference between the model shown in Fig. 6, *a* and the previous one (Fig. 2, *a*) is the use of four parallel aluminum cables with a cross section of 3×185 mm^2 in both sections, which results in

a significant reduction of power losses. The study of the influence of the main pumps DC drive on the operation of the electric network was carried out in four stages. In the first stage, the stray capacitance of the cable line was neglected, for which the Pi Section Line blocks of the mathematical model shown in Fig. 6, *a* were replaced with the corresponding Series RL Branch blocks, and there was no harmonic filtering and reactive power control device. In the second stage, the stray capacitance of the cable line was taken into account. In the third stage, the mathematical model was supplemented with the capacitor bank, and in the fourth stage with the harmonic filter, excess power reactor and automatic control system of reactive power of this reactor. In the first, second and third stages of the study, simulation of simultaneous starting of three pump units, and in the fourth stage, simulation of alternate and simultaneous starting of one, two, three and four pump units were performed.

4. 3. 1. Simulation results without taking into account the stray capacitance of the cable line

Fig. 9 presents the graphs of current and armature speed transients of three DC motors during their start-up to the rated speed of the 48D-22 pump.

The speed reference voltage of the double-circuit automatic control system is 10 V. Since the obtained graphs are the same, they are shown only for the pair of motors. As can be seen, the speed transient time is less than in the case of induction motor and does not exceed 5 s. This is due, in particular, to the fact that the MPE-1000-630 UKHL3 DC motor has a much smaller armature moment of inertia than the rotor moment of inertia of the AN16-41-12 motor. The speed overshoot is about 0.1 %, which is relatively small, since the set maximum value of the armature current of each motor is increased by only 20 % compared to the rated value. According to Fig. 9, the stationary armature speed value with high accuracy is equal to the specified one, and the peak-to-peak ripple amplitude of the quasi-steady-state armature current does not exceed 4 % of its rated value. The peak value acquired by the armature current during the transient is almost equal to the set maximum. The minimum firing angle reached during the start-up of the drives is close to 20 electrical degrees. Fig. 10 shows the diagram of thyristor converter input voltage and the resonance filter output signal.

It is seen that starting from the moment of 0.5 s, the converter input voltage is characterized by switching variations, which are absent in the filter output signal. Up to this point, the converter input voltage is sinusoidal. The filter output voltage is characterized by a shape that is similar to the input signal, but has a slightly smaller amplitude. Such a discrepancy does not have a significant effect on the simulation results, but can be reduced if necessary by increasing the relative accuracy of the calculation and, as a consequence, execution time. Referring to Fig. 11, *a*, it can be concluded that the relative deviation of the supply voltage of the three DC drives during their simultaneous start-up to the rated speed of the pumps does not exceed 4 %.

Even smaller relative deviation is characteristic of the secondary line voltage of the main transformer. The total current consumed by the TSZP-1600/10U3-1 transformers from the network is essentially non-sinusoidal, as evidenced by Fig. 11, *b*. The current diagram shown in this figure does not contain a dead time, which is fully consistent with the delta connection of the transformer secondary winding. If we consider Fig. 12, *a*, it can be assured that the secondary line voltage of the main transformer is also subject to switching variations. But their relative magnitude is significantly lower compared with the secondary voltage that feeds the thyristor converters.

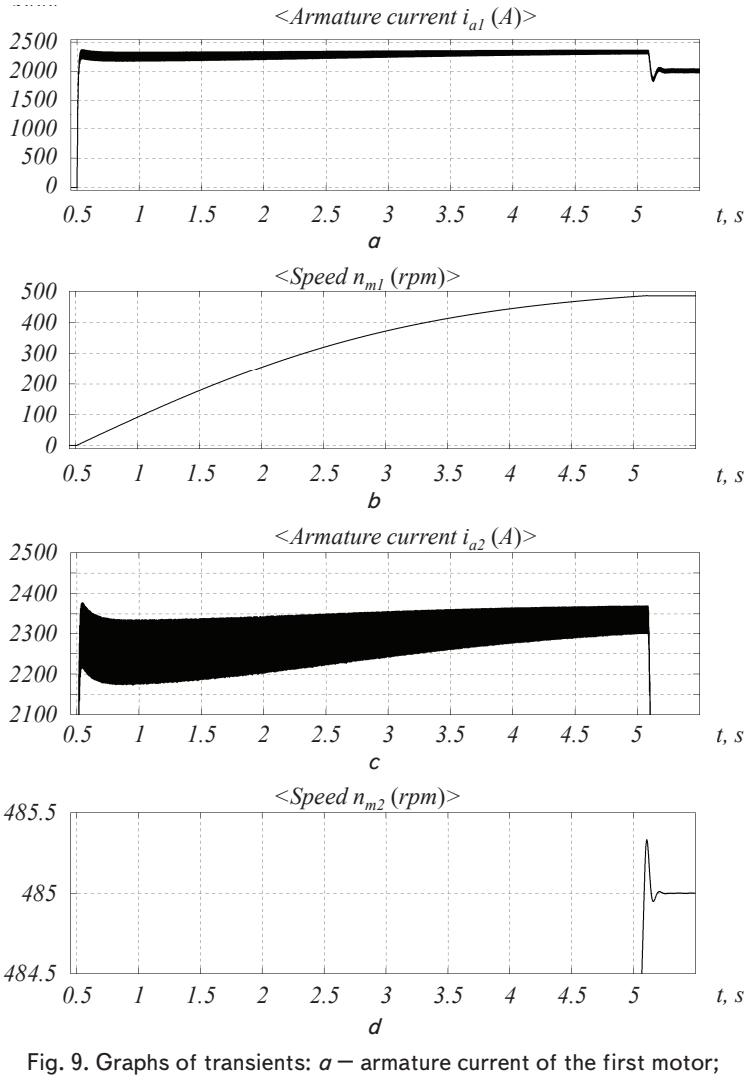

Fig. 9. Graphs of transients: *a* — armature current of the first motor; *b* — shaft speed of the first motor; *c* — armature current of the second motor; *d* — shaft speed of the second motor

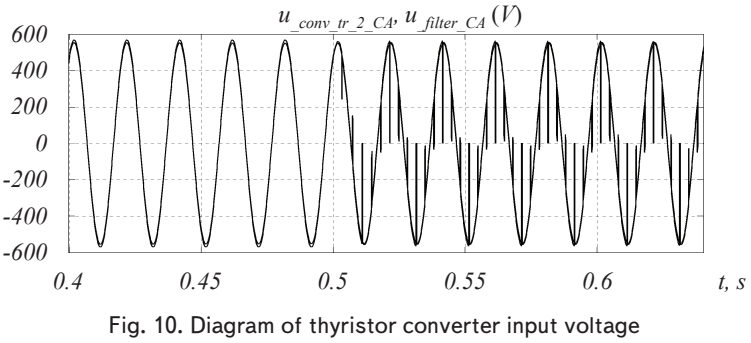

Fig. 10. Diagram of thyristor converter input voltage

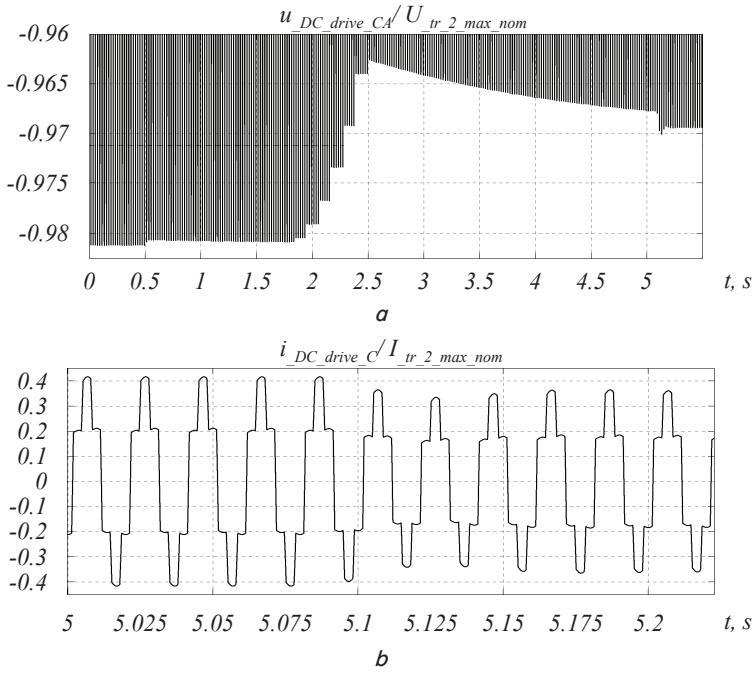

Fig. 11. Diagram: *a* — supply voltages of DC drives; *b* — total current consumed of drives

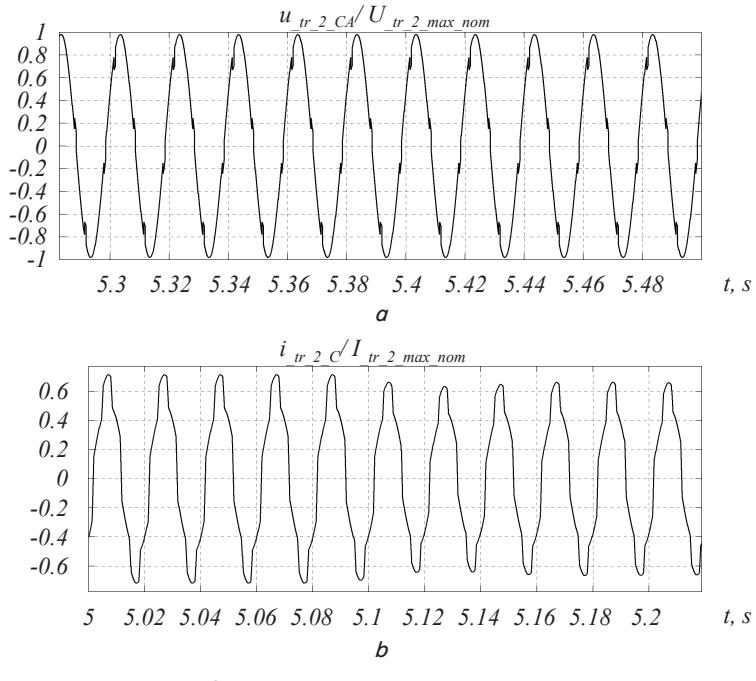

Fig. 12. Diagram: *a* — secondary line voltage; *b* — main transformer current

In accordance with Fig. 12, *b*, the secondary line current of the main transformer at the expense of other electric consumers is relatively smoother than in Fig. 11, *b*, but also has a pronounced non-sinusoidal character.

4. 3. 2. Simulation results taking into account the stray capacitance of the cable line

The study on the mathematical model showed that the stray capacitance of the cable line significantly affects the nature of physical processes taking place in the electric network with thyristor drives. This effect is negative because high-frequency voltage fluctuations occur in all cable line nodes during the operation of the power system. The amplitude of these fluctuations can reach values that are dangerous to electric equipment. So, Fig. 13 shows the diagram of the line voltage of the intermediate cable line node that exceeds the rated value by almost 1.5 times at the beginning of the transient.

The graphs of armature current and shaft speed transients of DC motors were similar to those shown in Fig. 9, and so are not given here. High-frequency fluctuations in the supply voltage of the TSZP-1600/10U3-1 transformers exist, both during the start-up and in the steady-state operation mode, as can be seen referring to Fig. 14, *a*.

Unlike the secondary line current of the main transformer, the diagram of the total line current consumed by the converter transformers from the network has no corresponding high-frequency component. This follows from the comparison of Fig. 14, 15, *b*.

In accordance with Fig. 15, *a*, the secondary line voltage of the main transformer at the beginning and end of the transient exceeds the rated value by more than 20 %. In the steady-state operation mode of electric pump units, the level of overvoltage at the main transformer output is more than 15 %. The analysis showed that the amplitude of high-frequency voltage fluctuations of the cable line nodes decreases with the decrease in the number of simultaneously operating electric pump units, but normal operating conditions of electric equipment may still not be ensured. To reduce the harmful effect of the cable line parasitic capacitance on the network, thyristor converters can be connected to transformers through additional current limiting reactors. However, this solution has drawbacks. Inductive resistance of the current-limiting reactors at the fundamental frequency is the value of the same order as the short-circuit reactance of transformers reduced to the number of secondary turns. Thus, the switching resistance will be substantially greater and the external characteristics of the converters will be much softer. Power consumption, mass dimensions and cost of electric drives will also increase accordingly.

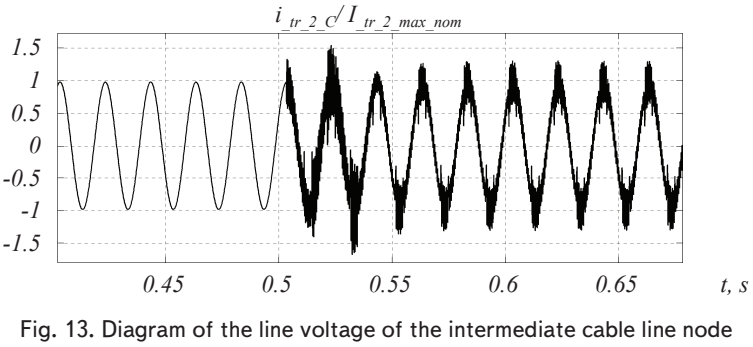

Fig. 13. Diagram of the line voltage of the intermediate cable line node

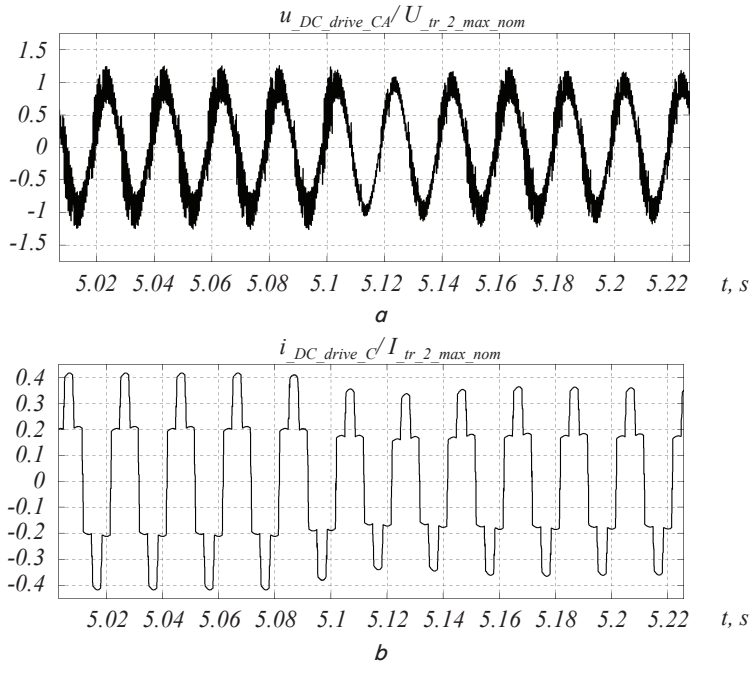

Fig. 14. Diagram: *a* — supply voltage of DC drives; *b* — total current consumedof drives

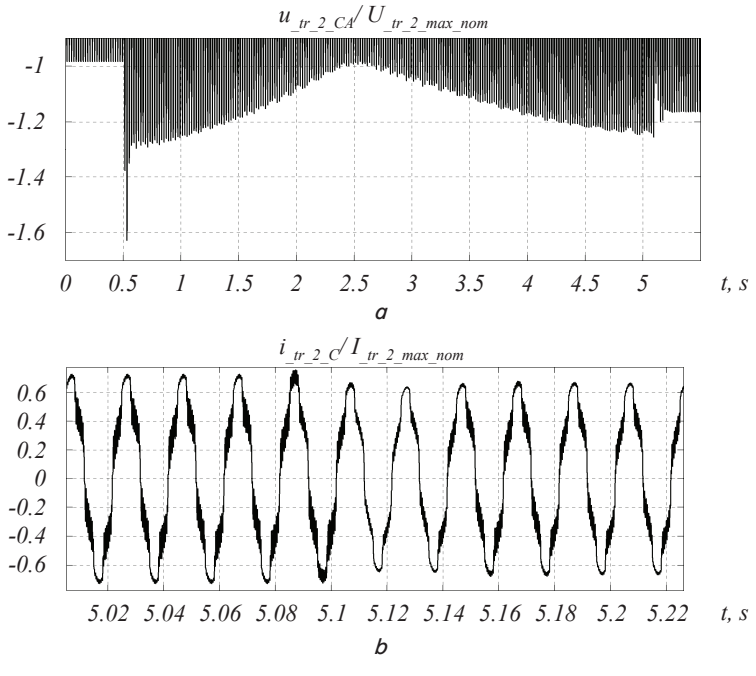

Fig. 15. Diagram: *a* — secondary line voltage; *b* — main transformer current

4. 3. 3. Simulation results with capacitor bank

At this stage, the mathematical model of the electric network includes thyristor drives, stray capacitance of the cable line and capacitor bank of installed capacity. Based on the obtained results, it can be ascertained that there are no high-frequency voltage fluctuations of the cable line nodes in all considered operating modes. The large capacity of the capacitor bank caused an increase in the amplitude value of the supply voltage of the TSZP-1600/10U3-1 transformers, as evidenced by Fig. 16, *a*.

As follows from Fig. 16, *a*, in no-load conditions of the transformers, the relative overvoltage is about 5 % compared to the rated value. During the transient process, this value reaches a maximum of approximately 9 %, and in statics decreases and remains at 1.5 %. The graphs of current and armature speed transients of DC motors are generally similar to those shown in Fig. 9. However, in this case, the maximum value of the armature current reached during start-up increased and exceeded the set point by approximately 3.3 %. The peak-to-peak ripple amplitude of armature current during quasi-steady-state operation increased to almost 6.3 % of the rated value. The thyristor firing angle during the transient was not lower than 30 electrical degrees. Because the capacitor bank constantly consumes reactive power from the network, the total current consumed by DC drives at idle has a value that even exceeds the quasi-steady-state.

This can be seen in Fig. 16, *b*. The figure also shows that a significant decrease in the total current is observed at the beginning of the start-up of motors, when there is a surge of reactive power consumed by thyristor converters. Fig. 17, *a* confirms the absence of high-frequency fluctuations in the supply voltage of TSZP-1600/10U3-1 transformers, but the nature of voltage variation over time is markedly non-sinusoidal.

An even greater deviation from the sine wave is characteristic of the diagram of total current consumption presented in Fig. 17, *b*.

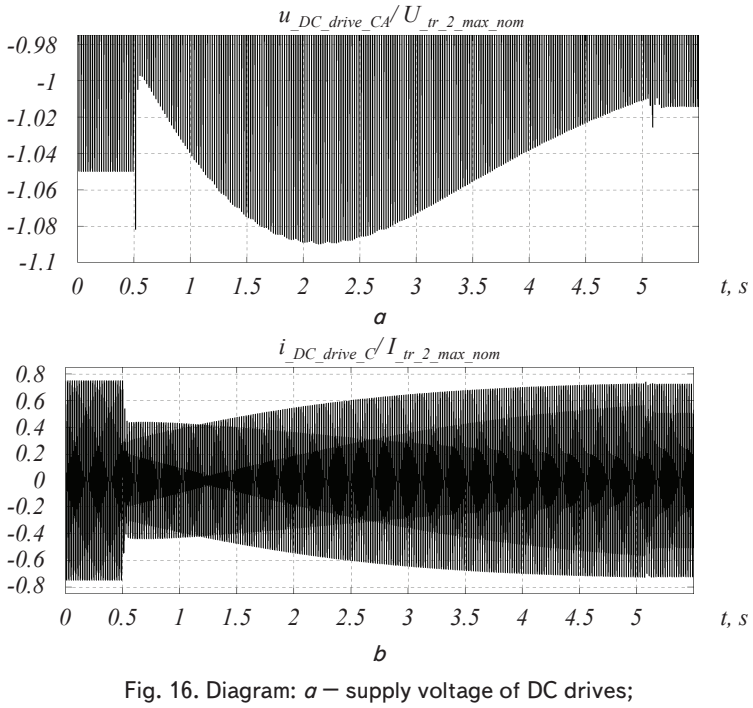

Fig. 16. Diagram: *a* — supply voltage of DC drives; *b* — total current consume of drives

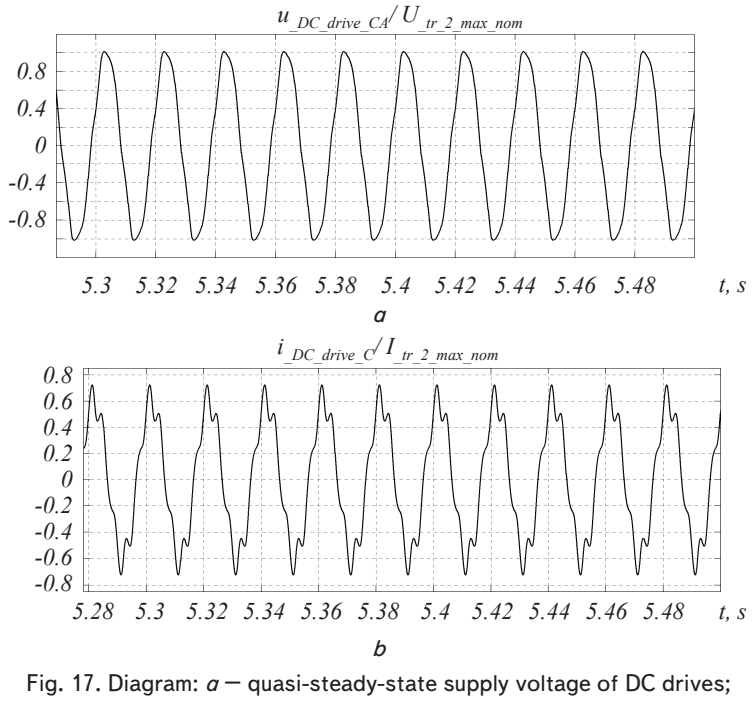

Fig. 17. Diagram: *a* — quasi-steady-state supply voltage of DC drives; *b* — total current consumedof drives

Comparative analysis of the diagrams of total current consumption in Fig. 14, *b* and Fig. 17, *b* allows us to conclude that the amplitude values of current for the two cases under consideration differ almost twice. This is due to the large capacity of the capacitor bank. However, reducing the capacity of the capacitor bank is not appropriate, as it leads to a greater deviation of voltage and current shape from the sinusoidal.

4. 3. 4. Simulation results with automatic harmonic filtering and reactive power control device

The mathematical model used during the fourth and last stage of the electric network simulation differs from the previous one by the presence of harmonic filter and automatic control system of excess reactive power. The analysis showed that due to the presence of adjustable harmonic filtering and reactive power control device, the conditions of joint operation of the electric network and DC drives are the most favorable. In this case, there are no high-frequency voltage fluctuations of the cable line nodes. In addition, reactive power consumption from the network is significantly reduced, as well as active power loss and voltage drop in some sections of the line. The waveform of voltage and total current consumed by DC drives from the network is the closest to the sine wave. It is also possible to generate reactive power into the network. The quality indicators of current and armature speed transients of DC motors are, as in the previous cases, at an acceptable level, as can be seen from Fig. 18.

The diagrams shown in Fig. 18, *a* correspond to the speed reference voltage of 3 V, and Fig. 18, *b* – 10 V. Both figures indicate that the number of simultaneously operating pump units does not significantly affect the nature of the transients. However, the amplitude of speed fluctuations at the end of the transient at 3 V is much higher than at the speed reference voltage of 10 V. This can be explained by the use of non-reversible voltage converter on the one hand and linear mode of the automatic control system on the other. At the speed reference voltage of 3 V, the quasi-steady-state motor armature current is continuous, but the operating mode approaches the maximum continuous.

From Fig. 18, *a* it follows that the peak value of the armature current during motor start-up exceeds the set maximum by about 1.1 %. At the speed reference voltage of 10 V, the value of the peak-to-peak ripple amplitude of the armature current in the quasi-steady-state mode does not exceed 4 % of the rated value, at a voltage of 3 V – 9 %. The firing angle in the quasi-steady-state operation mode of electric drives with the increase in the number of simultaneously operating pump units is slightly reduced, but remains significantly greater than 20 electric degrees. Fig. 19 shows the graphs of transients of reactive and active power of the reactor, as well as the total reactive and active power of DC drives.

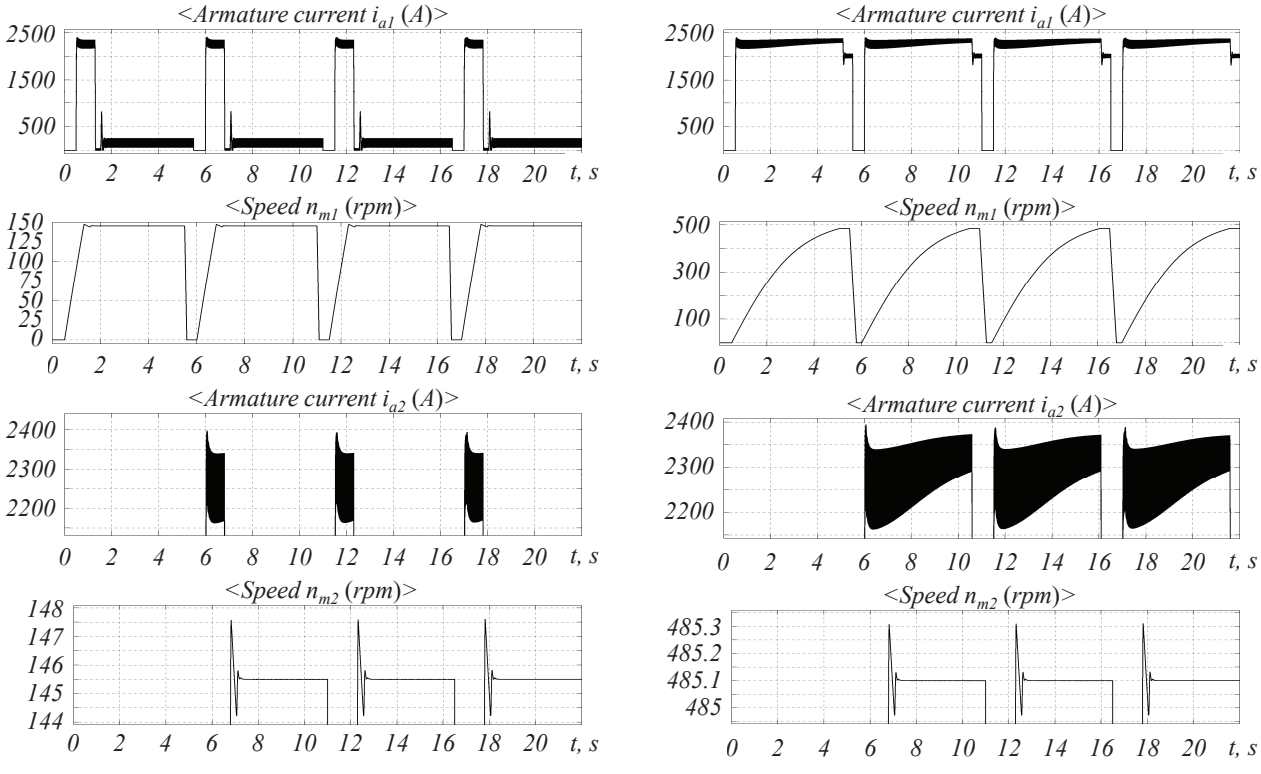

a *b*

Fig. 18. Graphs of transients of DC motors at the speed reference voltage: *a* – 3 V; *b* – 10 V

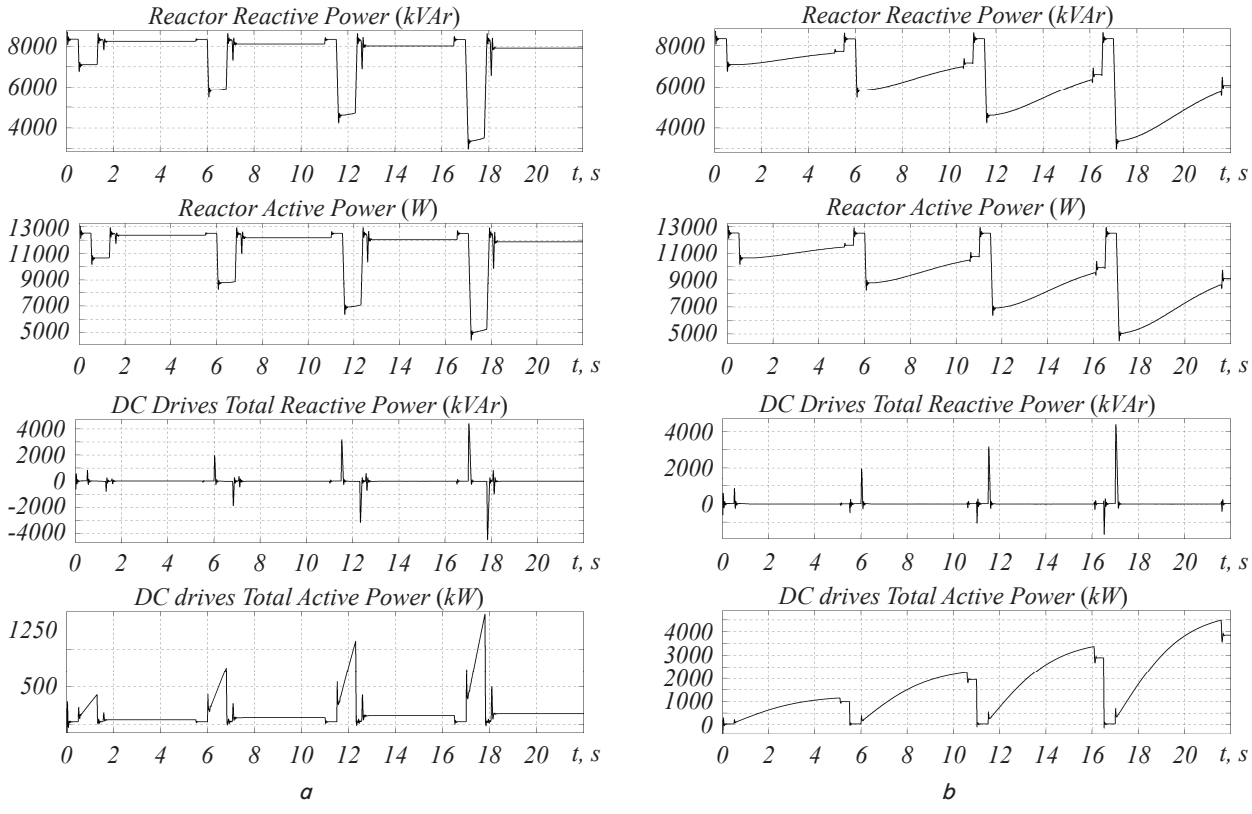

a *b*

Fig. 19. Graphs of power transients at the speed reference voltage: *a* – 3 V; *b* – 10 V

Fig. 19, *a* corresponds to the speed reference voltage 3 V, and Fig. 19, *b* – 10 V. Since the reactive power of the reactor far exceeds the active power, these values vary roughly in direct proportion. In Fig. 19, *a* it can be seen that a significant decrease in the reactive (active) power of the reactor occurs during each start-up, and with an increase in the

number of units, the reactor power consumption is reduced markedly. The reactor power variations at the beginning of each transient correspond to the surge of reactive power of parallel-connected DC motors.

The greatest reactive power variation is achieved with simultaneous operation of four pump units and is about 5,000 kVAr. The transients are accompanied by surges of the total reactive power of drives, since the rate of changes in the reactor reactive power is limited and the established value cannot be achieved instantly.

With the increase in the number of electric pump units, short-term variations in total reactive power become more intense.

If the number of electric drives is four, then the total reactive power in absolute magnitude at the beginning and at the end of start-up briefly exceeds 4,000 kVAr at the speed reference voltage of 3 V. And at the speed reference voltage of 10 V, the reactive power jumps at the end of the transient are significantly lower and with the number of electric pump units equal to four do not exceed the value of 500 kVAr. By comparing the diagrams of total active power consumption of electric drives, it can be concluded that with increasing the speed reference voltage from 3 V to 10 V, this value increases by more than an order of magnitude. This is explained by the fan nature of the load. The value of total active power consumption of DC drives does not take into account the power consumption of motor fields.

As follows from the diagram in Fig. 19, *b*, the total active power of the quasi-steady-state mode with increasing number of operating units increases not in direct proportion. This is because the total active no-load power of the four non-switched converter transformers, reactor and capacitor bank is not a value that depends on the number of units directly proportionally. Fig. 20 similar to Fig. 10 also indicates relatively large switching variations of instantaneous line voltage at the thyristor converter input.

As can be seen, there are no high-frequency voltage fluctuations that can be caused by the stray capacitance of the cable line. The output voltage of the resonance filter contains no variations and practically is in phase with the input voltage. The diagram of the input line voltage of TSZP-1600/10U3-1 transformers, Fig. 21, *a*, assures that, regardless of the number of units, the instantaneous voltage except for three short surges does not exceed the rated value of the secondary voltage of the main transformer.

Short-term voltage bursts occur as a result of self-induction EMF, which is induced in the armature coil when the thyristor control pulses are blocked at the beginning of motor braking. Fig. 21, *b* shows the diagram of the total line current consumed by DC drives, including the harmonic filtering and reactive power control device.

At the beginning of each start-up, there are short bursts of instantaneous current, which are comparable to the current value at the end of the transient and are caused by the finite performance of the automatic reactive power control system. Except for the initial sections, the current gradually increases during the transients. Depending on the number of operating pump units, the quasi-steady-state current value changes almost directly proportionally, reaching 40 % of the rated amplitude current of the main transformer when the number of units is four. Referring to Fig. 22, it can be seen that the shape of the diagrams of the secondary line voltage and current of the main transformer is much closer to sinusoidal than that of the similar diagrams shown in Fig. 12.

Some fleeting curvature of the current diagram occurs at the end of the transient, but does not have a significant effect on the electric network.

As shown in Fig. 23, the instantaneous line voltage of the intermediate cable line node at the beginning of the transient is briefly reduced by less than 7 %, which is better compared to unadjustable-speed induction motor.

Comparing Fig. 17, 24, we conclude that with harmonic filter and automatic reactive power control system, the voltage and current waveform becomes much closer to the sine wave.

It should be noted that in the first case, the number of operating pump units is three, and in the last case – four.

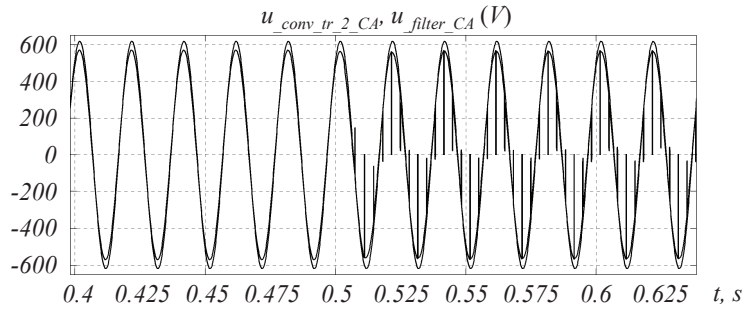

Fig. 20. Diagram of thyristor converter input voltage

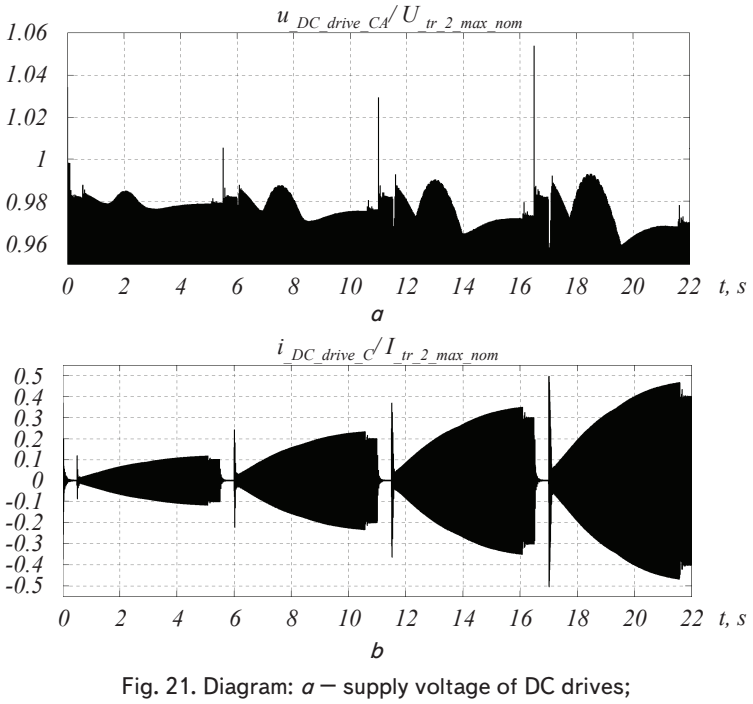

Fig. 21. Diagram: *a* – supply voltage of DC drives; *b* – total current consumption of drives

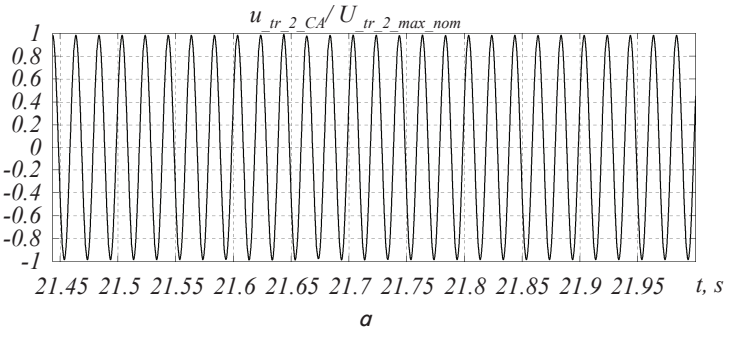

a

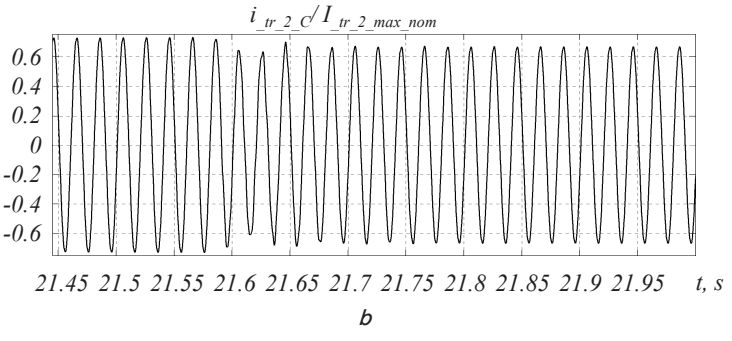

b

Fig. 22. Diagram: *a* — secondary line voltage; *b* — main transformer current

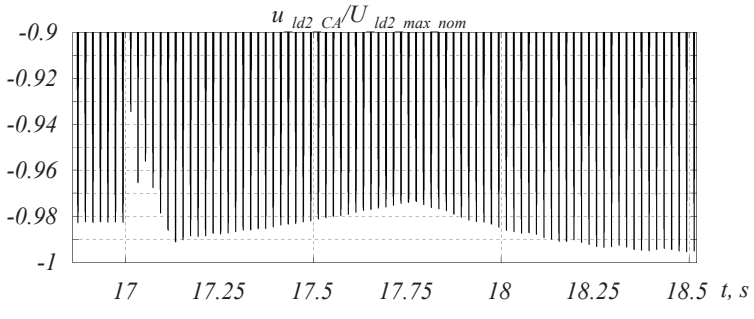

Fig. 23. Diagram of the line voltage of the intermediate cable line node

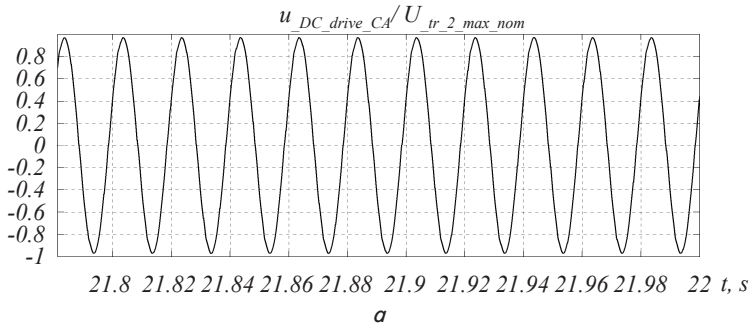

a

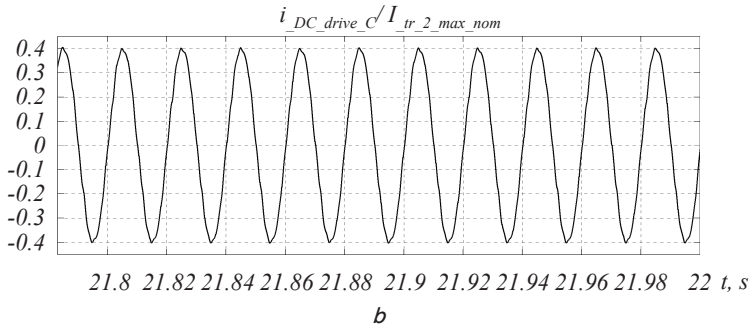

b

Fig. 24. Diagram: *a* — quasi-steady-state supply voltage of DC drives; *b* — total current consumedof drives

5. Discussion of the results of step-by-step modeling of the electric network with powerful DC drives

Summarizing the results of step-by-step mathematical modeling of the electric network, it can be concluded that only due to the capacitor bank, which is connected in parallel with converter transformers, it is possible to get rid of switching variations and high-frequency voltage fluctuations. This is evidenced by Fig. 17, *a*. High-frequency voltage fluctuations can occur due to the stray capacitance of the cable line and have the appearance as shown in Fig. 13, 14, *a*. However, the waveform of instantaneous voltage and total current consumed in this case differs significantly from the sine wave, as follows from Fig. 17. The total reactive power, which is characterized by the leading power factor, may be excessively large and may not meet the real needs of the electric network. As a consequence, the current and loss of active power of the cable line increase, and voltage deviation of its nodes from the rated can acquire critical values. This can be seen in Fig. 16. In the mathematical model, the block diagram of which is presented in Fig. 7, *a*, the capacitance of the capacitor bank was assumed as unchanged and corresponding to the simultaneous operation of four pump units. However, it is possible to raise the question of dividing the capacitor bank into four sections, which will be switched on depending on the number of operating pump units. Partitioning of the main elements of the harmonic filtering and reactive power control device is aimed at reducing the active power losses that occur in them, while disconnecting part of the pump units and improving the reliability of the electromechanical system as a whole. It is expedient to model such a system in the future. It is possible to significantly approximate the waveform of instantaneous voltage and total current consumed to the sine wave using the passive harmonic filter, tuned to the fifth and seventh current harmonics. The corresponding block is built into the subsystem shown in Fig. 7, *a*. If necessary, a second filter can be installed to suppress the eleventh and thirteenth current harmonics. This may be the subject of further research. Since the reactive power consumed by the filter at the fundamental harmonic is much lower than that of the capacitor bank, filter partitioning is less significant. To compensate for the excess reactive power, in which the reactor power of the capacitor bank overrides the total reactive power of the harmonic filter and DC drives, a reactor of the respective rated power must be installed. The reactor can consist of four parallel sections similar to the capacitor bank. However, in the proposed mathematical model, the reactor is described simply using the Three Phase Dynamic Load block shown in Fig. 7, *a*. This approach somewhat limits the scope of the results obtained. The mathematical model also has an automatic control system of the reactor reactive power,

which minimizes the total reactive power of electric drives and harmonic filtering and reactive power control device in static and dynamic modes. In real conditions, to reduce the cost of the electromechanical system, it is possible to refuse reactive power control and accept a constant reactor power, for example, equal to the reactive power of the capacitor bank. If reactive power control is more rational, then it can be implemented in several ways. On the one hand, it is possible to install a magnetically controlled shunt reactor, and on the other, a static Var compensator. It should also be noted that the minimum reactor reactive power that can be reached in static and dynamic modes is sufficiently large and is about 40 % of the maximum. This follows from the reactor power diagrams in Fig. 19. In view of this, the entire reactor, or each of its four sections, can be implemented as a parallel connection of conventional and adjustable parts, which will reduce the cost of the control system. If the reactive power control is limited only to static modes of drives, the cost of the control system can be reduced even more, since the range of changes in the reactor power will be reduced. But this will increase the negative impact of DC drives on the electric network during transients, which will lead to an increase in the total current consumed and voltage drop of the cable line nodes. This effect can be mitigated by reducing the starting currents of motors. It is possible to estimate the economic impact of the above measures by modeling in future research.

The results of the studies show that the replacement of unadjustable-speed induction motor drive of the drydock main pumps with adjustable-speed thyristor drive is feasible. This can significantly reduce the negative impact of the drive on the network.

6. Conclusions

1. For accurate simulation of AN-16-41-12 deep-bar induction motors, the own method for determining the viscous friction coefficient and T-shaped equivalent circuit parameters of the virtual motor in MatLab SimPowerSystems according to the catalog data is proposed. This method is based on formulas describing physical processes in the T-shaped circuit except for the rated and critical moment formulas that correspond to the specified L-shaped equivalent circuit.

In the virtual induction motor block, constant losses can only be accounted for by the viscous friction coefficient undividedly. In order to improve the accuracy of the model, it was proposed to introduce the corrected values of the initial starting and critical torque ratio into the calculation.

Because the catalog data set of the induction motor is overridden, the rated power factor is calculated from other motor data, followed by a comparison of the result obtained with the specified value.

The dependences of rotor resistance on slip in this work are approximated by relatively simple elementary functions, which provide almost constant values of these parameters at subcritical slip values.

The mathematical model of the short-circuited induction motor with a round-slot rotor was implemented using the block of the wound-rotor induction motor, to the rotor winding terminals of which the variable active-inductive load is applied. Two other similar motors, which are already started, are described by virtual squirrel-cage induction motor blocks, with the equivalent circuit parameters corresponding to the rated operation mode.

2. The simulation showed that, even with the alternate starting of the pump units, there is a significant voltage drop at the stator winding terminals, which increases during starting each subsequent unit. If the fourth electric pump unit is in reserve, then the most difficult conditions are characteristic of starting the third electric pump unit, when the first two operate in steady-state mode against a closed discharge valve of pressure water pipes. According to the results of the simulation, during starting the third electric pump unit, which lasts more than 8 s, the line voltage drop of the intermediate cable line node is 8...10 %.

3. The mathematical model of DC drives was built with a common automatic control system of armature speed for all electric pump units. The principle of subordinate control of electric drive coordinates is used, and only one DC motor has feedback of the armature current and speed.

At the input of each synchronized 6-pulse generator of the respective voltage converter, there is a resonance filter tuned to transmit harmonics with network frequency. This eliminates operating errors caused by switching variations or high-frequency voltage fluctuations of the input line.

The results of the step-by-step mathematical simulation show that without the harmonic filtering and reactive power control device, there are switching variations (in absolute magnitude – drops) of line voltage at all cable line nodes during the operation of DC drives. The current consumed from the network is substantially non-sinusoidal, and also reactive power is consumed from the network.

If the stray capacitance of the cable line is additionally taken into account in the mathematical model, then high-frequency line voltage fluctuations occur in all cable line nodes. This creates unsafe conditions for electric equipment, as instantaneous voltage may take excessively high values in absolute magnitude.

4. With the capacitor bank, the possibility of high-frequency voltage fluctuations in the cable line nodes caused by stray capacitance is eliminated. But the waveform of voltage and total current consumed by electric drives is significantly different from a sine wave. Also, a significant amount of reactive power is generated into the network, and the voltage of the line nodes may significantly exceed the rated value.

5. By installing proper harmonic filtering and reactive power control device, all of these negative effects can be eliminated, and the automatic reactive power control system may be advantageous to minimize reactive power consumption. This system controls the reactor reactive power, which compensates for the excess total reactive power of DC drives, capacitor bank and harmonic filter.

The maximum power of the simulated reactor exceeds the established useful power of four DC drives about 2.4 times.

Acceptable transient quality in the total reactive power control circuit was achieved with the integrated variable gain reactor power controller. Among other things, the controller performs the function of limiting the rate of changes in the reactor power at a predetermined level.

At the simultaneous starting of four electric pump units, equipped with DC motors, against a closed discharge valve of pressure pipes with a total duration of less than 5.5 s, the drop of the line voltage of the intermediate cable line node is 3...7 %.

In the mathematical model, a single harmonic filtering and reactive power control device is used, although in real conditions it can be rationally divided into several parallel sections, which helps to increase reliability and reduce active power consumption by the electromechanical system from

the network. Depending on the control method and range, the reactor of excess reactivity may consist of parallel connection of the regulated and unregulated parts.

Thus, the influence of unadjustable-speed AC drive and adjustable-speed thyristor drive of the drydock main pumps on the electric network of the Okean shipyard was investigated using the detailed mathematical model built in MatLab SimPowerSystems. It is shown that AC drive can be replaced with DC drive, but using the harmonic filtering and reactive power control device.

References

1. Grigor'ev, V. N., Marchenko, D. V., Simakov, G. V., Smelov, V. A. (1976). Sudospusknye i sudopodemnye sooruzheniya (proektirovanie i stroitel'stvo). Leningrad: Stroyizdat, 176.
2. Bugaev, V. T., Dubrovskiy, M. P., Yakovlev, P. I., Shtefan, A. V. (2001). Konstruktsiya suhih dokov i ih vzaimodeystvie s gruntom. Moscow: OOO «Nedra-Biznestsentr», 372.
3. Hristo, P. E. (2015). Energy-saving control of a dry dock dewatering pumps. Electrotechnic and computer systems, 19 (95), 154–159. doi: https://doi.org/10.15276/eltecs.19.95.2015.36
4. Khristo, P. (2018). Experimental study into optimal interdependence of energy-time costs for emptying a dry dock. Eastern-European Journal of Enterprise Technologies, 4 (2 (94)), 35–55. doi: https://doi.org/10.15587/1729-4061.2018.139674
5. Neyman, Z. B., Pekne, V. Z., Moz, L. S. (1974). Krupnye vertikal'nye ehlektrodvigateli peremennogo toka. Moscow: Energiya, 376.
6. Talib, M. H. N., Ibrahim, Z., Rahim, N. A., Hasim, A. S. A. (2013). Characteristic of Induction Motor Drives Fed by Three Leg and Five Leg Inverters. Journal of Power Electronics, 13 (5), 806–813. doi: https://doi.org/10.6113/jpe.2013.13.5.806
7. Singh, B., Kumar, G. (2008). Battery Energy Storage System Based Controller for a Wind Turbine Driven Isolated Asynchronous Generator. Journal of Power Electronics, 8 (1), 81–90.
8. Jo, G.-J., Choi, J.-W. (2018). A Novel Method for the Identification of the Rotor Resistance and Mutual Inductance of Induction Motors Based on MRAC and RLS Estimation. Journal of Power Electronics, 18 (2), 492–501. doi: https://doi.org/10.6113/JPE.2018.18.2.492
9. Wang, M., Wang, D., Dong, G., Wei, H., Liang, X., Xu, Z. (2019). Simplified Rotor and Stator Resistance Estimation Method Based on Direct Rotor Flux Identification. Journal of Power Electronics, 19 (3), 751–760. doi: https://doi.org/10.6113/JPE.2019.19.3.751
10. Sivokobylenko, V. F., Pavlyukov, V. A. (1979). Raschet parametrov shem zameshcheniya i puskovyh harakteristik glubokopaznyh asinhronnyh mashin. Elektrichestvo, 10, 35–39.
11. German-Galkin, S. G. (2001). Komp'yuternoe modelirovanie poluprovodnikovyh sistem v MATLAB 6.0. Sankt-Peterburg: KORONA print, 320.
12. Chernyh, I. V. (2008). Modelirovanie ehlektrotehnicheskih ustroystv v MATLAB, SimPowerSystems i Simulink. Moscow: DMK Press; Sankt-Peterburg: Piter, 288.
13. Tuganov, M. S. (1978). Sudovoy beskontaktnyy ehlektroprivod. Leningrad: Sudostroenie, 288.
14. Jannati, M., Idris, N. R. N., Aziz, M. J. A. (2016). Performance Evaluation of the Field-Oriented Control of Star-Connected 3-Phase Induction Motor Drives under Stator Winding Open-Circuit Faults. Journal of Power Electronics, 16 (3), 982–993. doi: https://doi.org/10.6113/jpe.2016.16.3.982
15. Zhu, R.-W., Wu, X.-J. (2014). Simplified SVPWM that Integrates Overmodulation and Neutral Point Potential Control. Journal of Power Electronics, 14 (5), 926–936. doi: https://doi.org/10.6113/jpe.2014.14.5.926
16. Sun, C., Ai, S., Hu, L., Chen, Y. (2015). The Development of a 20MW PWM Driver for Advanced Fifteen-Phase Propulsion Induction Motors. Journal of Power Electronics, 15 (1), 146–159. doi: https://doi.org/10.6113/jpe.2015.15.1.146
17. Daigavane, M., Suryawanshi, H., Khan, J. (2007). A Novel Three Phase Series-Parallel Resonant Converter Fed DC-Drive System. Journal of Power Electronics, 7 (3), 222–232.
18. Singh, B., Bist, V. (2013). Improved Power Quality IHQRR-BIFRED Converter Fed BLDC Motor Drive. Journal of Power Electronics, 13 (2), 256–263. doi: https://doi.org/10.6113/jpe.2013.13.2.256
19. Klyuchev, V. I. (2001). Teoriya elektroprivoda. Moscow: Energoatomizdat, 704.
20. Kolesnik, G. P. (2017). Kabel'nye i vozdushnye linii ehlektroperedachi. Vladimir: Vladim. gos. un-t, 126.
21. Azarh, D. N.; Zelenova, S. P., Eyfelya, A. I. (Eds.) (1953). Nasosy. Katalog-spravochnik. Moscow: Gos. Nauch.-teh. izd. mash.-stroit. i sud.-stroit. lit., 428.
22. Bulhar, V. V. (2006). Teoriya elektropryvodu. Odessa: Polihraf, 408.
23. Kravchik, A. E., Shlaf, M. M., Afonin, V. I., Sobolenskaya, E. A. (1982). Asinhronnye dvigateli serii 4A. Moscow: Energoizdat, 504.
24. Gaysarov, R. V., Shchelkonogov, A. E., Kayukov, S. I., Loktyushin, K. N. (2004). Spravochnik po vysokovol'tnomu oborudovaniyu ehlektroustanovok. Versiya: 2.0. Yuzhno-Ural'skiy gosudarstvennyy universitet.
25. Eliseev, V. A., Shinyanskiy, A. V. (Eds.) (1983). Spravochnik po avtomatizirovannomu ehlektroprivodu. Moscow: Energoatomizdat, 616.
26. Kopylov, I. P., Klokov, B. K. (Eds.) (1988). Spravochnik po ehlektricheskim mashinam. Vol. 2. Moscow: Energoatomizdat, 456.
27. Evzerov, I. H., Gorobets, A. S., Moshkovich, B. I. et. al.; Perel'muter, V. M. (Ed.) (1988). Kompletnye tiristornye ehlektroprivody. Moscow: Energoatomizdat, 319.
28. Gerasimyak, R. P. (1992). Povyshenie kachestva sistem avtomaticheskogo upravleniya. Kyiv: UMK VO, 100.
29. Zimenkov, M. G., Rozenberg, G. V., Fes'kov, E. M. (Eds.) (1983). Spravochnik po naladke ehlektrooborudovaniya promyshlennyh predpriyatiy. Moscow: Energoatomizdat, 480.